University of Rhode Island

DigitalCommons@URI

2021

SIMULATION METHODS FOR WOVEN FABRIC MATERIALS SUBJECTED TO BIAXIAL LOADING

Felix N. Klempt
University of Rhode Island, felix_klempt@uri.edu

SIMULATION METHODS FOR WOVEN FABRIC MATERIALS SUBJECTED

TO BIAXIAL LOADING

BY

FELIX N. A. KLEMPT

A THESIS SUBMITTED IN PARTIAL FULFILLMENT OF THE

REQUIREMENTS FOR THE DEGREE OF

MASTER OF SCIENCE

IN

MECHANICAL ENGINEERING

UNIVERSITY OF RHODE ISLAND

2021

MASTER OF SCIENCE THESIS

OF

FELIX N. A. KLEMPT

APPROVED:

Thesis Committee:

Major Professor   David G. Taggart

Helio Matos

George Tsiatas

Brenton DeBoef

DEAN OF THE GRADUATE SCHOOL

UNIVERSITY OF RHODE ISLAND

2021

ABSTRACT

The rising demand in inflatable structures gives rise to the need to accurately predict the non-linear behavior of the woven skin material of these structures. The simulations which are in place right now often oversimplify the behaviour of the fabric, not using the full potential woven fabrics or inflatable structures could have.

This research aims to develop a tool with which a variety of different fabrics can be modelled and simulated to let a designer explore different kind of materials and yarns before making a decision on which fabric to use without the need for extensive laboratory experiments.

In order to do so, three dimensional models are constructed using the TexGen program designed by the University of Nottingham. These models are based on a 1000 denier fabric which is tested experimentally parallel to this thesis. The result of the experimental tests is then used in an effort to refine and verify the models.

It is shown that these models vastly depend on the yarn properties. Even properties that would be expected to have a minor influence on the overall fabric behavior like transverse and shear properties are crucial for the accuracy of the model. Despite the fact that the model as it stands cannot predict the behavior of the fabric as accurately as necessary to use it as a tool to design new fabrics, it is a first step in the development of such a tool.

ACKNOWLEDGMENTS

Far too many people helped me in the last year to in my studies at the University of Rhode Island and in the completion of my Masters thesis to list them all in this section. I am grateful for the help and advises I received regarding my thesis directly and indirectly. Although I cannot list every person, there are some people I want to acknowledge formally.

First of all I want to thank my major advisor Professor Taggart for all the guidance throughout my thesis. Prof. Taggart was always accessible for every question I had in my research. With his proficiency in computational mechanics he supported my research heavily. I learned a lot of about research in the field of modeling and simulation is conducted.

Next I would like to acknowledge the members of the research group for thoughtful advise every week. Professor Tsiatas, Tjard, Matt, Anthony and Rogan always had new ideas to try out when I encountered problems. I want to give my special thanks to Matt, Rogan and Anthony for providing me with the experimental results necessary for the completion of this thesis.

Next I would like to thank my house and new found friends in America who made me feel at home from the first day and to whom I could go and explain my thoughts when I encountered difficulties even though the topic may not be interesting to them.

Lastly I want to say thank you to my family and friends back at home who were always there for me when things got stressful, listening to my complaints. Especially I want to thank my parents who made this exchange possible. Thank you.

TABLE OF CONTENTS

LIST OF FIGURES

LIST OF TABLES

CHAPTER 1

Introduction

1.1 Motivation

For the last decade, inflatable woven fabric structures became very popular due to their exceptional mechanical properties [1]. These mechanical properties offer the ability to optimize constructions regarding performance, cost, manufacturability and repairability. Other properties like weight minimization together with rapid and self deployment and a large deployed-to-packed-ratio offer unparalleled functionality especially in marine and space applications where weight and space requirements are critical [2, 3]. Additionally woven structures are drapeable and allow for complex structures to be formed [4].

The design process of inflatable structures, on the other hand, is beset by unique material related challenges which cannot be found in traditional materials. Since fabrics are made out of interlocked yarns with voids between them, they are heterogeneous in nature and do not deform as a continuum [3]. The interlocking of the yarns also introduces nonlinearities into the material in the form of friction and decrimping of the yarns during deformation. The weave has a natural undulation structure which, under load, tends to straighten [4]. The complicated weave pattern of the yarns also make it difficult to analyze local and global mechanical behaviors in woven textiles [5]. All of these difficulties and nonlinearities make it challenging to develop constitutive equations that accurately describe the behaviour of woven fabrics. Material testing using multiaxial stresses is essential for full characterization of material behaviour [6]. Simulations which are in place right now are often simplified and can lead to a more conservative view on the load carrying capabilities of woven fabrics [1].

An ability to accurately estimate the effective elastic properties is an impor-

tant step in designing and analyzing materials [7]. Accurate prediction methods would reduce the amount of material testing needed to identify appropriate weave constructions for specific applications.

1.2 Goals of the Research

This research aims to develop a finite element model in order to accurately predict the mechanical response of woven fabric materials subjected to uniaxial and biaxial in-plane loads. It will be validated by experimental data collected parallel to this research. The model has the ability to be modified to allow for the investigation of different yarn materials and weave patterns of the woven fabric. Once an accurate prediction of the mechanical response is calculated, these results will be correlated with a netting analysis. The results from this thesis can be implemented into a laminate model which itself can be used for designing inflatable structures constructed with woven fabric skins [2].

1.3 Methodology

In the following thesis, the buildup of a three dimensional Finite Element Model is discussed. In the upcoming chapter 2, several theoretical topics will be discussed which make up the the foundation of this study. These topics include the basics of woven structures in itself, biaxial testing and elastic material properties. The chapter also describes the theory behind both modeling techniques, the Finite Element Method and the Netting Analysis. The used program TexGen and the homogenization method are also explained.

Chapter 4.3 describes how the experiments which accompanied this research are carried out. It is also explained what the results of these experiments are and how they tie in with this thesis.

The actual modelling is described in detail in chapter 3. First the netting

analysis is conducted, afterwards the three dimensional model is designed. This designing process is described in order that future research can be conducted using this thesis as a guide to develop a model of their own. The models are then validated and evaluated in chapter 4.

The final chapter concludes the thesis and gives recommendation on what topics to focus in future research to deepen the findings in this thesis.

List of References

[1] J. Gager and H. Pettermann, "Fem modeling of multilayered textile composites based on shell elements," *Composites Part B: Engineering*, vol. 77, pp. 46–51, 2015.

[2] A. M. Alich, "Modeling, simulation and investigation of inflatable drop-stitch panels with finite element analysis," Master's thesis, University of Rhode Island (URI), 2019.

[3] P. V. Cavallaro, A. M. Sadegh, and C. J. Quigley, "Decrimping behavior of uncoated plain-woven fabrics subjected to combined biaxial tension and shear stresses," *Textile Research Journal*, vol. 77, no. 6, pp. 403–416, 2007.

[4] K. Buet-Gautier and P. Boisse, "Experimental analysis and modeling of biaxial mechanical behavior of woven composite reinforcements," *Experimental mechanics*, vol. 41, no. 3, pp. 260–269, 2001.

[5] R. Misra, A. Dixit, and H. S. Mali, "Finite element (fe) shear modeling of woven fabric textile composite," *Procedia materials science*, vol. 6, pp. 1344–1350, 2014.

[6] Y. Hanabusa, H. Takizawa, and T. Kuwabara, "Numerical verification of a biaxial tensile test method using a cruciform specimen," *Journal of Materials Processing Technology*, vol. 213, no. 6, pp. 961–970, 2013.

[7] S. L. Omairey, P. D. Dunning, and S. Sriramula, "Development of an abaqus plugin tool for periodic rve homogenisation," *Engineering with Computers*, vol. 35, no. 2, pp. 567–577, 2019.

CHAPTER 2

Theoretical Foundation

2.1 Woven Structures

Woven structures are the most commonly used technical textiles in engineering due to their good suitability for a variety of applications and well balanced properties such as the ease of handle, good drape-ability and reduced manufacturing cost [1]. Fabrics are made up out of individual yarns, which itself are made up of thin fibers at the micro level. These yarns are most of the times woven together in a two dimensional weave where two sets of yarns lie at right angles to each other. The yarns that run along the length of the fabric are called warp yarns or ends. The yarns which run perpendicular to them from side to side are called weft yarns or picks. [2]

The different fabric properties like strength, extensibility, porosity and durability can be influenced. The most influential parameters are the yarns per centimeters (thread spacing), the structure of the raw material and the linear density and twist factor of the yarns. Some combinations of these parameters can provide vastly different properties in weave and weft direction. Although here are practically unlimited weaving structures possible the most prominent are plain, twill, satin and basket from which the plain weave is the most common one [2, 1]. The plain weave is the simplest interlacing pattern in which each warp yarn is alternating between lifting over and going under the weft thread. A plain weave is shown in Figure 1. This kind of weave has the most intersections between weft and warp yarns per unit area [2]. In some fabrics the amount of weft and warp yarns differ from one another. For a warp-faced plain weave the warp cover factor is higher than the weft cover factor. There are more yarns in the warp direction. This results in a higher weft crimp [2]. An extreme example of the resulting higher cover
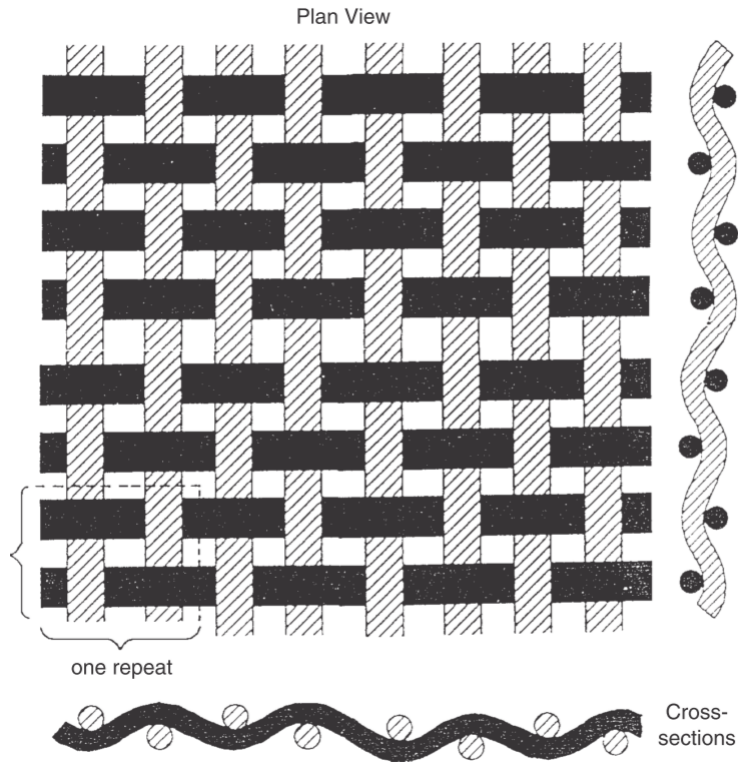
Figure 1: Fabric woven with plain weave and warp and weft cross sections [2]

factor can be seen in Figure 2. The lightly colored warp yarns have considerably higher undulation then the almost straight black weft yarns. This undulation or waviness of the yarn is called crimp. It is created by the weaving process itself in which the different yarns are forced to bend around each other thus cannot lay straight in the woven fabric [2].

The interactions between the yarns at the fabric level is another factor which greatly influences the overall behaviour of the fabric [1]. At the micro scale the slip resistance of individual fibers is the most dominant factor influencing the yarn interaction. At the meso scale the dominant factor becomes the yarn trellising and the rotation at the crossover points.
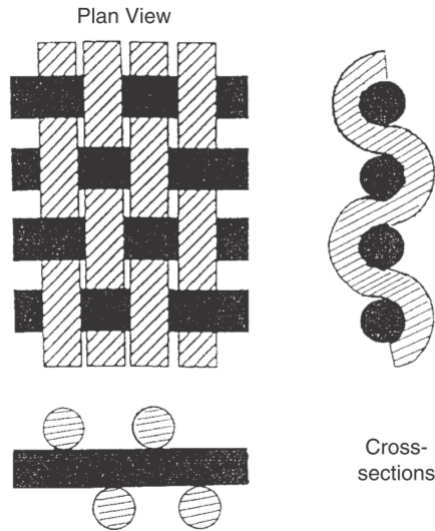
Figure 2: Plain weave with substantially higher warp than weft cover factor [2]

2.2 Biaxial Testing

A biaxial test or two-axial tensile test, is used to investigate the response of different materials subjected to loading in two directions. Biaxial testing machines consist of two perpendicular actuators. The biaxial testing machine is made up of four jaws, two of which are parallel to each other. Each pair of jaws can be controlled separately. This configuration allows for a simultaneous application to different loads in two perpendicular directions and complex load cases histories can be created. [3]. Such a machine is depicted in Figure 3 conducting a uniaxial test. The specimen (green circle) is held in place by two of the jaws. In a biaxial test the perpendicular jaws would load the specimen in both directions.

Complete characterization of woven fabrics require a plane biaxial test since the forces can be introduced independently in the two main directions [4]. In woven fabrics a biaxial test is needed to determine the material properties when subjected to various combinations of axial and transverse stressing [4, 3]. Load in one direction always influences the material response in the perpendicular direction [3].
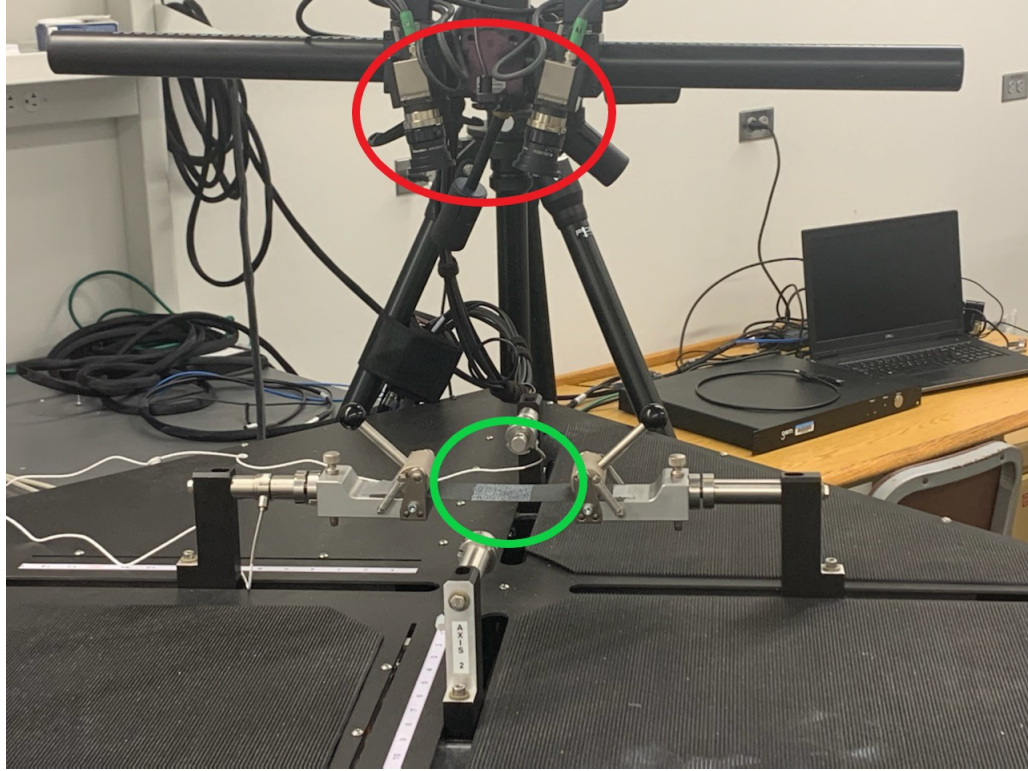
Figure 3: Biaxial testing machine conducting a uniaxial test.

Biaxial testing for woven fabrics is currently coincided to be the only testing method to accurately characterize the mechanical response of coated fabrics and foils. It can be used to investigate material properties, of fabrics with different fibers or weaving patterns. The fabric sample is pulled in weave and weft direction at the same time through force, strain or displacement control. The fabric specimen is elongated at a constant rate. Different ratios of the load in warp and weft are possible. During biaxial elongation the required forces in each direction are recorded. If the testing machine is calibrated correctly and the principal directions of the material align, the center of the woven fabric sample remains stationary [4].

2.2.1 Digital Image Correlation (DIC)

Digital Image Correlation (DIC) is a non-contact optical method to measure strain and displacement. It is more accurate than manual measurement methods

while being cost effective [5]. A camera setup records the deformation of the specimen as it is loaded. The camera system can be seen in Figure 3, indicated by a red circle. In the most basic setting the camera takes two pictures, one before and one after deformation. These pictures are then digitized, stored and compared to one another to calculate strain and displacement. The computer program compares one well defined area from the undeformed sample with the deformed one. This area is called a subset. Often times the subset is painted with an artificial random dot pattern. The dot pattern has a high contrast in points which helps the program finding matching subsets before and after deformation [6]. The comparison of the two subsets is shown in the following Figure 4. From this information the program
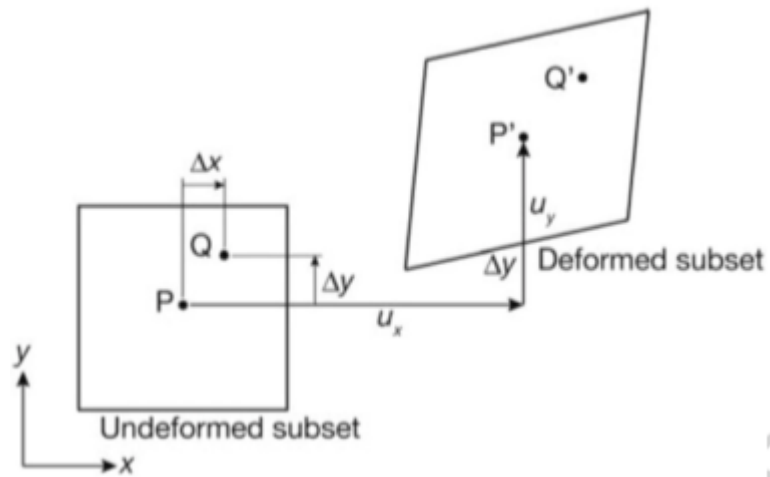
Figure 4: Subset before and after deformation [6]

calculates the strain and displacement of the specimen. Chu et al. [7] give a more detailed explanation of the digital correlation method including a discussion of the image analysis algorithm used to compute displacement and strain fields.

2.3 Elastic Material Properties

Constitutive equations describe macroscopic material response with phenomenological or constitutive variables such as stress, strain and temperature [8]. In the following chapter the constitutive equations for a linear elastic solid is de-

rived. The mechanical behavior of solids usually is defined by constitutive stress-strain relations where stress as a function of strain, strain rate, strain history and material properties [9]. For the study, it is assumed that neither the strain rate nor the strain history has an impact on the deformation of the solid when subjected to quasi-static loading. The strain of the solid is assumed to depend only on the applied stress and the material properties. Furthermore, a linear material response is assumed in the deriving of the constitutive equations. The linear response ends in each material at the proportional limit. Up until this point, if a load is removed, the sample returns in its original shape and the strain disappears. Under small deformations, many materials exhibit linear elastic behavior. The consecutive equations for a one dimensional axial loading case is

$$\sigma = E\varepsilon \tag{1}$$

where σ is the stress, ε is the strain and E is the slope of stress-strain curve. E is also known as Young's modulus. Equation 1 is known as Hooke's Law [9]. Based on the assumption that for three-dimensional stressing, each stress component can be expressed as a linear combination of each strain component. For a fully anisotropic material, these relations can be expressed in matrix form as

$$\begin{Bmatrix} \sigma_x \\ \sigma_y \\ \sigma_z \\ \tau_{xy} \\ \tau_{yz} \\ \tau_{zx} \end{Bmatrix} = \begin{bmatrix} C_{11} & C_{12} & C_{13} & C_{14} & C_{15} & C_{16} \\ C_{21} & C_{22} & C_{23} & C_{24} & C_{25} & C_{26} \\ C_{31} & C_{32} & C_{33} & C_{34} & C_{35} & C_{36} \\ C_{41} & C_{42} & C_{43} & C_{44} & C_{45} & C_{46} \\ C_{51} & C_{52} & C_{53} & C_{54} & C_{55} & C_{56} \\ C_{61} & C_{62} & C_{63} & C_{64} & C_{65} & C_{66} \end{bmatrix} \begin{Bmatrix} \varepsilon_x \\ \varepsilon_y \\ \varepsilon_z \\ 2\varepsilon_{xy} \\ 2\varepsilon_{yz} \\ 2\varepsilon_{zx} \end{Bmatrix} \tag{2}$$

C_{ij} are material parameters called elastic moduli with the unit of stress (force/area) and the factor 2 is required to maintain symmetry of the [C] matrix. This relation can be expressed in tensor notation as

$$\sigma_{ij} = C_{ijkl}\varepsilon_{kl} \tag{3}$$

where C_{ijkl} is a fourth-order tensor whose 81 components describe all material parameters necessary to characterize the material. Due to symmetry these 81 components can be reduced to 36 independent ones. With the inclusion of strain energy leads to the relation $C_{ij} = C_{ji}$ and the independent components reduce again to a total of 21 [9]. The elastic tensor for a completely anisotropic material can now be written as

$$
\begin{bmatrix}
C_{11} & C_{12} & C_{13} & C_{14} & C_{15} & C_{16} \\
 & C_{22} & C_{23} & C_{24} & C_{25} & C_{26} \\
 & & C_{33} & C_{34} & C_{35} & C_{36} \\
 & & & C_{44} & C_{45} & C_{46} \\
 & Sym. & & & C_{55} & C_{56} \\
 & & & & & C_{66}
\end{bmatrix}
\tag{4}
$$

For special materials the elastic tensor can further be reduced. For orthotropic materials for example the total amount of independent elastic moduli is 9. An orthotropic material is a material with three mutually perpendicular planes of symmetry. It can be seen that with a mirror reflection on three perpendicular planes of symmetry gives

$$
C_{i4} = C_{j5} = C_{k6} = 0 \ (i = 1, 2, 3; \ j = 1, 2, 3, 4; \ k = 1, 2, 3, 4, 5)
\tag{5}
$$

[9]. Thus the linear elastic constitutive equation of an orthotropic material is given by

$$
\begin{Bmatrix}
\sigma_x \\
\sigma_y \\
\sigma_z \\
\tau_{xy} \\
\tau_{yz} \\
\tau_{zx}
\end{Bmatrix}
=
\begin{bmatrix}
C_{11} & C_{12} & C_{13} & 0 & 0 & 0 \\
C_{12} & C_{22} & C_{23} & 0 & 0 & 0 \\
C_{13} & C_{23} & C_{33} & 0 & 0 & 0 \\
0 & 0 & 0 & C_{44} & 0 & 0 \\
0 & 0 & 0 & 0 & C_{55} & 0 \\
0 & 0 & 0 & 0 & 0 & C_{66}
\end{bmatrix}
\begin{Bmatrix}
\varepsilon_x \\
\varepsilon_y \\
\varepsilon_z \\
2\varepsilon_{xy} \\
2\varepsilon_{yz} \\
2\varepsilon_{zx}
\end{Bmatrix}
\tag{6}
$$

The material parameter C_{ij} are commonly expressed in terms of the engineering constants which directly relate to physical properties of the material. Engineering constants can be interpreted as the material's ability to resist deformation. Young's modulus as seen in equation 1 for the 1D case is the resistance of the material in

compression or tension to axial stress. The index corresponds to the direction of the resistance. The shear modulus G is the material's resistance to shear deformation. Equivalent to Hooke's Law it links the shear stress τ with the tangent of the shear angle γ in the plane indicated by the indices. Equation 7 shows the relationship between these quantities.

$$\tau_{ij} = G_{ij}\gamma_{ij} \tag{7}$$

Deformations perpendicular to the direction of elongation can be described by the ratio of elongation in two directions and is called the Poisson's ratio ν_{ij}, where i is the direction of the applied stress and j is the direction in which the transverse contraction is measured. Usually the second subscript is perpendicular to the direction of the applied stress. The following Equation 8 shows how the Poisson's ratio can be determined.

$$\nu_{ij} = -\frac{\varepsilon_{jj}}{\varepsilon_{ii}} \tag{8}$$

With nine the independent engineering constants $E_1, E_2, E_3, G_{12}, G_{13}, G_{23}, \nu_{12}, \nu_{13}$ and ν_{23} equation 6 can be rewritten as [10]

$$\begin{Bmatrix} \sigma_x \\ \sigma_y \\ \sigma_z \\ \tau_{xy} \\ \tau_{yz} \\ \tau_{zx} \end{Bmatrix} = \begin{bmatrix} \frac{1-\nu_{23}\nu_{32}}{E_2 E_3 \Delta} & \frac{\nu_{21}+\nu_{31}\nu_{23}}{E_2 E_3 \Delta} & \frac{\nu_{31}+\nu_{21}\nu_{32}}{E_2 E_3 \Delta} & 0 & 0 & 0 \\ & \frac{1-\nu_{13}\nu_{31}}{E_1 E_3 \Delta} & \frac{\nu_{32}+\nu_{12}\nu_{31}}{E_2 E_3 \Delta} & 0 & 0 & 0 \\ & & \frac{1-\nu_{12}\nu_{21}}{E_1 E_2 \Delta} & 0 & 0 & 0 \\ & & & G_{23} & 0 & 0 \\ & \text{Sym.} & & & G_{31} & 0 \\ & & & & & G_{12} \end{bmatrix} \begin{Bmatrix} \varepsilon_x \\ \varepsilon_y \\ \varepsilon_z \\ 2\varepsilon_{xy} \\ 2\varepsilon_{yz} \\ 2\varepsilon_{zx} \end{Bmatrix} \tag{9}$$

where

$$\Delta = \frac{1 - \nu_{12}\nu_{21} - \nu_{23}\nu_{32} - \nu_{13}\nu_{31} - 2\nu_{13}\nu_{21}\nu_{32}}{E_1 E_2 E_3}. \tag{10}$$

In order for orthotropic materials to stay stable, E_1, E_2, $E_3 > 0$ and $\nu_{21}\nu_{12}$, $\nu_{23}\nu_{32}$, $\nu_{13}\nu_{31} < 1$ must be satisfied. The additional Poisson's ratio can also be calculated by using the following relations between Young's modulus and Poisson's ratio.

$$\frac{E_1}{\nu_{12}} = \frac{E_2}{\nu_{21}}, \frac{E_1}{\nu_{13}} = \frac{E_3}{\nu_{31}}, \frac{E_2}{\nu_{23}} = \frac{E_3}{\nu_{32}} \tag{11}$$

12

2.4 Finite Element Method

A vast number of engineering problems can be described analytical by partial differential equations. All continuum mechanics, fluid mechanic problems or calculations of electrical fields fall into this category. The analytical partial differential equations is defined for every of the infinite points in space. Since a computer can only handle a finite amount of variables, it is necessary to reduce the infinite variables in the analytical equations to a finite number. This reduction of variables is called discretization [11].

The Finite Element Method is a very versatile method to discretize continuum problems. In contrast to other methods it can be used for arbitrary geometries. To discretize the geometry, the method divides the domain in smaller geometrically simple regions. These smaller simpler regions are called elements. Since there is a finite number of these elements, the method is called the Finite Element Method. The solution is then approximated by assumed interpolation functions within each element. For a sufficient number of elements the solution approaches the true solution [11]. The division of the problem in many simpler ones means the numbers of equations which needs to be solved increases significantly. Thus the computational power of computer is linked to the ability to solve these equations in a timely manner [12].

The Finite Element Method is suitable to solve mechanical problems with complex geometries, loading conditions and materials, even if an analytical solution cannot be obtained [12]. To solve such a complex problem several steps are necessary. In the following these steps as seen in Table 1 will be discussed. Some steps can be done by the user in cooperation with the computer these steps will be indicated with a $\star$-symbol. Other steps are solely done by the computer. These steps will be indicated with a $\diamond$-symbol.

1	Definition of the problem
2	Definition of the issue to be investigated
3	Determine the type of problem
4	⋆ Mesh generation and choice of element
5	⋄ Set up the system of equations
6	⋄ Computation of element loads
7	⋄ Solving the system of equations
8	⋄ Calculation of dependant variables
9	⋄ Output of the results
10	⋆ Evaluation of the results
11	Check for plausibility and choice of mesh
12	Answer the issue

Table 1: Steps of Finite Element Analysis [11]

In step one the problem is defined. To define the problem the geometry, applied loads, boundary conditions and material parameters have to be established. The second step, the definition of the issue, is an essential step in every computer simulation. Every user should be aware of the goal of the simulation. The more precisely the goal is formulated, the more successful is the simulation. In addition to the goal, the desired precision of the solution should also be determined since numerical simulations are an approximation. Since different problems could need different types of analytical models, the type of the problem has to be determined. Problems can either be static, if acceleration and inertia effects can be neglected. They also can be either linear, if increased load results in a proportional increased result, or nonlinear if the load and the result are not proportional to one another. Additionally the dimensionality and the symmetry can simplify the problem. In the next step the mesh and the element has to be defined. The user has to decide on an appropriate element to be used in the discretization. This decision is crucial for the accuracy of the simulation. Different element types allow for different types of interpolation such as linear or quadratic polynomials. After the problem and simulation approach is defined, the computer sets up the system of equations. In

step six the load cases are calculated and distributed to the respective elements. Subsequently the system of equation is solved. This system of equations solves for displacements, which are used to compute strain and stress fields. The stress-strain relationship of elastic material is described with constitutive equations derived in section 2.3. Most of the computation takes place in this step. Afterwards the dependant variables such as reaction forces are calculated. The computed results as well as the dependant variables can be saved for further analyses. In the post processing steps, the results are evaluated. Special programs allow for the display of stress distribution or graphs of all calculated variables. The calculated results should always be checked for plausibility. Results should be validated by comparison with a known problem or with experimental data. The chosen mesh should also be evaluated. A too course mesh will result in an inaccurate solution. The last step is to answer the question asked in step two [11, 12].

2.4.1 Derivation of the Finite Element Method

In the following section the principles of the Finite Element Method are derived mathematically. It will be shown how you can discretize the partial differential equations describing the continuum with the principle of virtual work. In a given volume in which all forces are in equilibrium the forces across the volume V and the surface S have to add up to zero. In the following equation the forces in the surface are denoted $\mathbf{t}$ and the forces in the volume $\mathbf{f}$.

$$\int_S \mathbf{t} \, dS + \int_V \mathbf{f} \, dV = 0 \tag{12}$$

The strain tensor $\boldsymbol{\sigma}$ is given by $\mathbf{t} = \sigma \cdot \mathbf{n}$, where $\mathbf{n}$ is the normal vector, thus

$$\int_S \boldsymbol{\sigma} \cdot \mathbf{n} \, dS + \int_V \mathbf{f} \, dV = 0. \tag{13}$$

With the Divergence theorem the surface integral can be turned into a volume integral:

$$\int_V \boldsymbol{\nabla} \cdot \boldsymbol{\sigma} \, dV + \int_V \mathbf{f} \, dV = \int_V (\boldsymbol{\nabla} \cdot \boldsymbol{\sigma} + \mathbf{f}) \, dV = 0 \tag{14}$$

Since this equation is valid for every volume, it has to be fulfilled point by point. The partial differential equation

$$\boldsymbol{\nabla} \cdot \boldsymbol{\sigma} + \mathbf{f} = 0 \tag{15}$$

has to be fulfilled for a material in equilibrium at every point. To solve it the external forces as well as the material parameters have to be determined. Since this equation is valid at infinite points it's not suitable to be solved by a computer. The concept of virtual displacement is used. Equation 15 is multiplied by an arbitrary test function $\delta \mathbf{v}$. Every point in the material is moved by $\delta \mathbf{v}(\mathbf{x})$. The resulting equation

$$(\boldsymbol{\nabla} \cdot \boldsymbol{\sigma}(\mathbf{x}) + \mathbf{f}(\mathbf{x})) \cdot \delta \mathbf{v}(\mathbf{x}) = 0 \tag{16}$$

is then integrated over the volume V to obtain

$$\int_V (\boldsymbol{\nabla} \cdot \boldsymbol{\sigma} + \mathbf{f}) \cdot \delta \mathbf{v}(\mathbf{x}) \, dV = 0. \tag{17}$$

The test function can be any function. Since it is a vector function it can be interpreted as displacement or velocity. In the FE-Method a function is chosen which is zero everywhere but on one element. The test function tests if the condition $\boldsymbol{\nabla} \cdot \boldsymbol{\sigma} + \mathbf{f} = 0$ is true at the tested element. Since the condition is only tested integrative it is called a weak equilibrium. The more test functions are chosen the better is the condition tested. With N test functions a set made out of N equations is obtained. With the chain rule equation 16 can be rearranged to

$$\boldsymbol{\nabla} \cdot (\boldsymbol{\sigma} \cdot \delta \mathbf{v}) = (\boldsymbol{\nabla} \cdot \boldsymbol{\sigma}) \cdot \delta \mathbf{v} + \sigma \cdot \cdot (\boldsymbol{\nabla} \otimes \delta \mathbf{v}). \tag{18}$$

Inserted in equation 17 and with the divergence theorem

$$\int_S \mathbf{t} \cdot \delta\mathbf{v} \, dS + \int_V \mathbf{f} \cdot \delta\mathbf{v} \, dV = \int_V \boldsymbol{\sigma} \cdot \cdot (\boldsymbol{\nabla} \otimes \delta\mathbf{v}) \, dV \tag{19}$$

is obtained. For a small displacement the virtual strain $\delta\varepsilon = (\boldsymbol{\nabla} \otimes \delta\mathbf{v} + (\boldsymbol{\nabla} \otimes \delta\mathbf{v})^T)/2$ can be inserted and the fundamental equation of FE-Method with small displacements is obtained:

$$\int_S \mathbf{t} \cdot \delta\mathbf{v} \, dS + \int_V \mathbf{f} \cdot \delta\mathbf{v} \, dV = \int_V \boldsymbol{\sigma} \cdot \cdot \delta\varepsilon \, dV \tag{20}$$

The equation for $\delta\epsilon$ is here only the symmetrical part of $\boldsymbol{\nabla} \otimes \delta\mathbf{v}$ since it's going to be multiplied with the symmetric vector $\boldsymbol{\sigma}$ the anti symmetric part will vanish [11].

To define the test function a form function $N_n(\mathbf{x})$ is chosen to restrict the possible displacements. The form function and the displacement at a certain point in space define as a linear combination the displacement. The displacement function is shown in equation 21. The index n numbers the form function.

$$\mathbf{u}(\mathbf{x}) = \sum_n \mathbf{u}_n N_n(\mathbf{x}) \tag{21}$$

For the test function the same depiction is used. This choice is known as the *Galerkin-Choice.*

$$\delta\mathbf{v}(\mathbf{x}) = \sum_n \delta\mathbf{v}_n N_n(\mathbf{x}) \tag{22}$$

The form function determines on the one hand where and in which way the test function is tested and it also describes the displacement function. Only displacements which can be expressed through equation 21 are valid.

2.4.2 Element Types

As stated in the previous section, the choice of the elements is an important part in solving a Finite Element Analysis. Abaqus, the Finite Element program

used in this thesis, offers a range of different elements. The element name is characterized by five features. Their family, degrees of freedom, number of nodes, formulation and integration [13]. The first letter of an elements tells which family it belongs to. Figure 5 shows commonly used element families. The letter S for
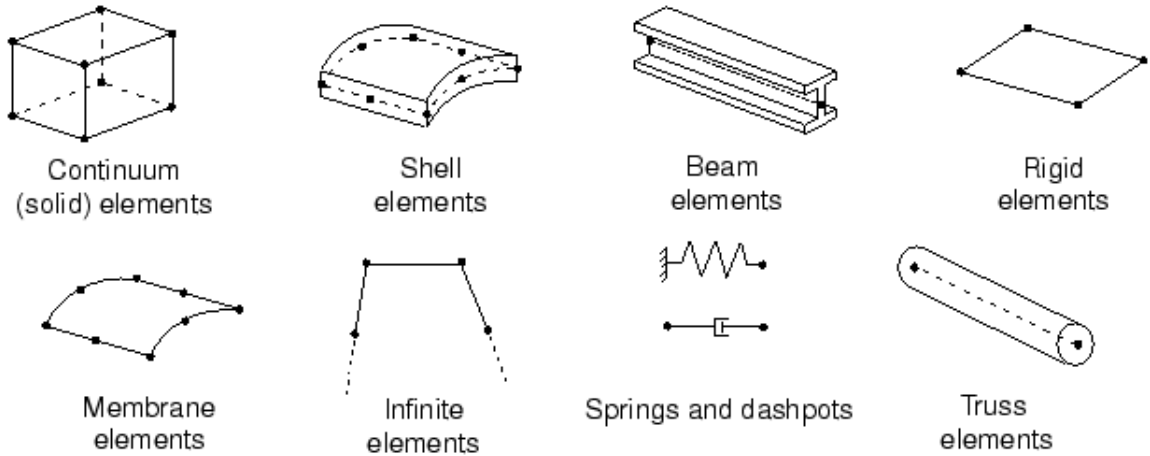
Figure 5: Commonly used element families [13]

example indicates a shell element, the letter C a solid element. The degrees of freedom are directly related to the element family. In a stress analysis the degrees of freedom are the translation in each direction. Some elements such as beam and shell elements also have rotational degrees of freedom. For a heat transfer analysis the temperature at each node as an additional degree of freedom is needed. Hence heat transfer analysis require different elements than stress analysis. In the element naming convention the degrees of freedom are not directly specified but implied by the family and the dimension of element. The dimension is specified directly after the family as *3D* or *2D* with the exception for shell and beam elements which do not specify the dimension [13].

Variables in the FE-Method are only calculated at the node of the element. In between the nodes in the element values are obtained by interpolation of the values at the nodes. The order of interpolation is determined by the amount of nodes

used in the element. Figure 6 shows different elements with different amounts of nodes. First order or linear interpolations are used with elements who only

(a) Linear element
(8-node brick, C3D8)

(b) Quadratic element
(20-node brick, C3D20)

(c) Modified second-order element
(10-node tetrahedron, C3D10M)
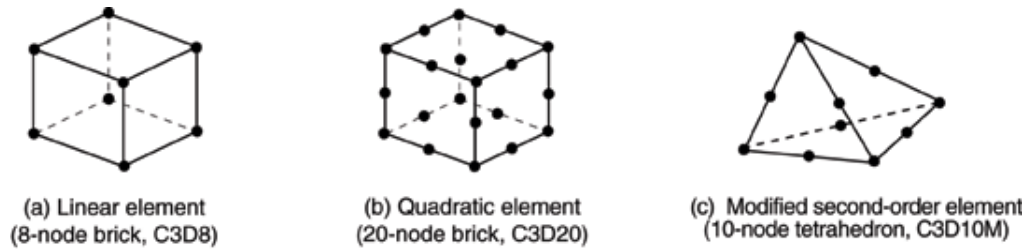
Figure 6: Linear brick (a), quadratic brick (b) and modified tetrahedral elements (c) [13]

have nodes at the corner (see figure 6 (a)). These elements are called first order or linear elements. Elements with nodes on the side as seen in figure 6 (b) are called quadratic elements since the interpolation between the nodes is quadratic. Modified second order elements, such as the tetrahedral element in figure 6 (c) are interpolated by a modified second order interpolation [13].

The formulation describes the mathematical theory used in the definition of the element. In the Lagrangian description the material associated with an element the material cannot leave the element. This type of description is used in stress and displacement problems. In the Eulerian or spatial description the material can flow through the elements which are fixed in space. This model is used in fluid and heat analysis [13]. Elements with an H at the end are hybrid elements. Elements which begin with an $\mathbf{C}$ and end with an T are multi purpose elements which have both mechanical and thermal degrees of freedom [13].

Some elements in Abaqus can use both full and reduced integration. This choice can have a huge impact on the simulation results. The reduced integration elements are indicated with and R at the end [13].

In this thesis Continuum elements are used. The elements used C3D8, C3D8R and C3D6 which are three dimensional brick or triangular prism elements with re-

duced integration and hourglass control, except for C3D8 which is fully integrated. These elements have three degrees of freedom. The nodes can be displaced in all three spacial directions.

2.5 Netting Analysis

A simple tool for approximating axial stresses in a composite material is the netting analysis. This type of analysis assumes that only the fibers are carrying load. The matrix is neglected in this regard and only holds the fibers in place. Bending, shear or discontinuity as well as resistance to buckling cannot be depicted in a netting analysis. The linear stress strain relationship is just Hooke's Law as in Equation 1. Transverse and shear moduli and stresses are considered to be zero [14].

A netting analysis is a quick and easy tool to get a good first estimate of the material or geometric properties of the examined part [14].

2.6 TexGen

TexGen is an open source software package developed at the University of Nottingham [15]. It is designed to model 2D and 3D geometries of textiles at the level of a unit cell [16]. A unit cell is the smallest section of a structure which, when repeated can replicate the structure as a whole due to periodic boundary conditions. Typically a unit cell ranges from several millimeters to centimeters in size. These unit cells are build up from yarns in a self supporting structure [16]. With this approach TexGen can model the mesoscale of a fabric material. In the mesoscale the yarns and their interaction such as the weaving patterns or friction are modelled [16].

The yarns are modelled as a full volume of a homogeneous material, not as individual fibers. They are considered as orthotropic bodies with the 1-direction

20
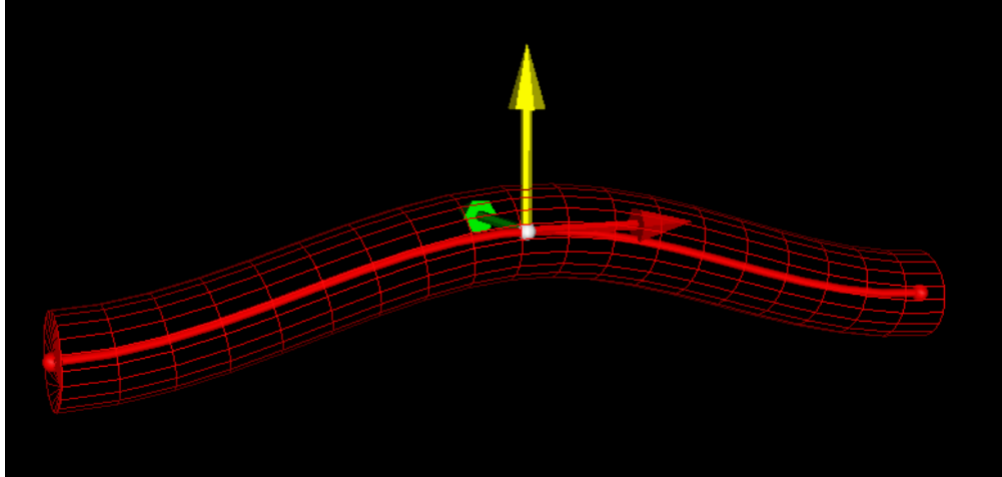
Figure 7: Center line of a yarn [15]

pointing in the direction of the yarn and the 2- and 3-directions perpendicular to the 1-direction. In Figure 7 the red arrow indicates the 1-direction and the yellow and green arrows indicate the 2- and 3-direction. The yarns 3D stiffness matrix consists of nine independent constants as discussed in section 2.3. This approach makes the modeling process easier, since the simulation of every fiber would be computational very expensive [1]. TexGen can calculate the yarn geometry with only the yarn path and the cross section of the yarn. The yarn path is characterized by a series of vectors which represent the yarn center line. The center line is a one dimensional line in three dimensional space lying directly in the center of each yarn. An example of such a center line is shown in Figure 7.

Along the center line discrete points, so called Master Nodes, are chosen. The interpolation between the nodes has at least the continuity of C^1 to avoid gaps in the yarn path and make the tangent to the yarn path vary smoothly. To interpolate spline functions are used. These functions are defined piece wise from one Master Node to the next one by polynomials [15, 16].

To maintain a continuity across the yarns in the adjacent unit cell the interpolation has to be periodic. The difference of a natural spline and a periodic

spline with the same knots is shown in figure 8. To create the yarn from the yarn
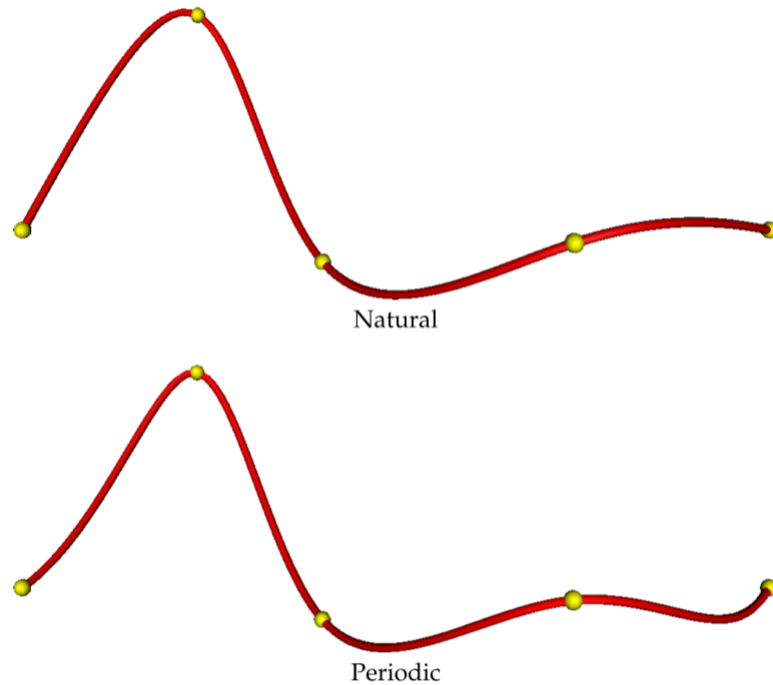
Natural

Periodic

Figure 8: Natural and periodic cubic splines [16]

path the cross section is modeled and swiped along the yarn path [16]. The cross section is a two dimensional shape lying perpendicular to the yarn path. It can be described by parametric equations in two dimensions. Cross sections are generally convex and can take on a variety of shapes. TexGen supports ellipses, lenticular shapes, power ellipses, hybrid shapes, rectangles and polygons. Power ellipses are slightly modified ellipses where the y coordinate is assigned a power n to change the shape of the ellipse to a rectangle with rounded edges for $n < 1$ or to a more lenticular shape for $n > 1$. For $n = 1$ there is no difference between a power ellipse and an ellipse. A lenticular shape is the intersection of two circles which are have an vertical offset where neither the offset nor the radii of both circles has to be the same. In Figure 9 both shapes are shown with different parameters. Figure 9a shows a more rectangular shape with the power $n = \frac{1}{2}$ on top and a more lenticular

(a) Power elipse   (b) Lenticular shape

Figure 9: Cross section of power ellipse and lenticular shapes with different parameters [16]

shape with a power of $n = 2$ below. Figure 9b shows a lenticular shape with two circles with the same radii but with no offset d on top and an offset of $d = \frac{h}{4}$ on the bottom. The de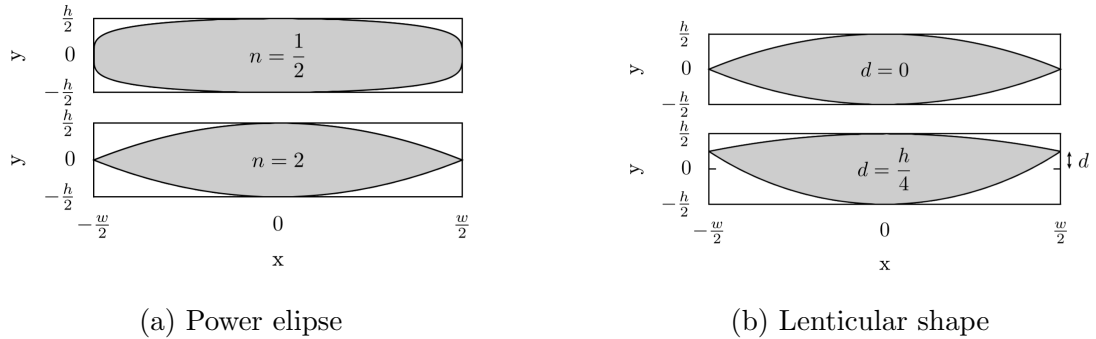fault is a constant cross section along the whole yarn path but if needed, the cross section can change between nodes or positions. The yarn in between those defined positions is interpolated [16].

The meshing in TexGen is done in two steps. In the first step the cross sections are meshed in two dimensions. This ensures that the cross section meshes are compatible. The second step links the adjacent cross section meshes together to form 3D elements. To mesh the cross section in a regular grid in the first step a simple meshing algorithm has been implemented [16].

TexGen allows for a wide variety of different weaves and textiles to be modelled accurately [16]. The easiest weave type is the plain weave. The plain weave consists of two layers of yarns. The amount of yarns in warp and weft directions as well as the yarn spacing and width and the fabric thickness can be manually entered. Both layers can be rotated against each other to model an even greater variety of plain weaves. Each yarn can additionally be selected to go over or under another yarn. Another possibility of creating weaves are 3D weaves. Those are weaves where binder yarns are binding different layers of the weaves together. These three

dimensional weaves were not used in this research, for more information on these types of weaves the website [15] and the program itself offer further information.
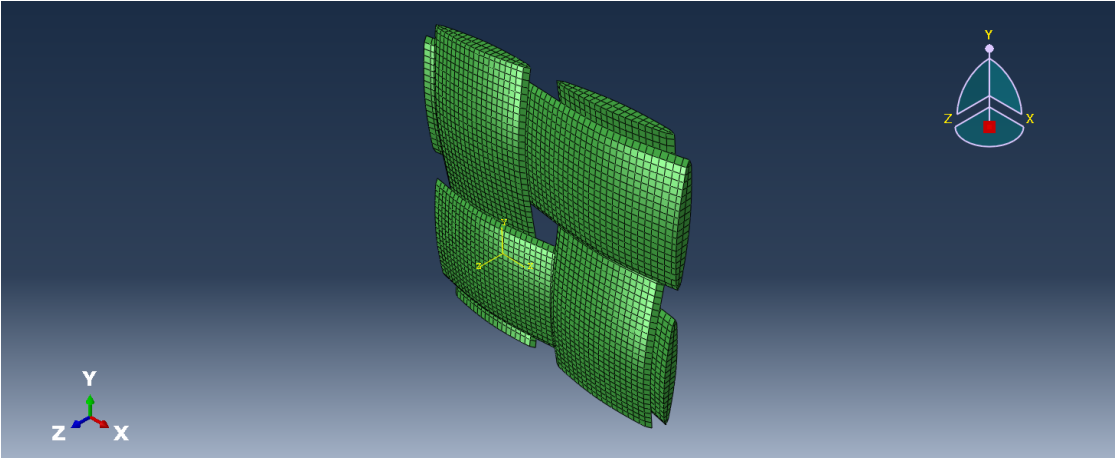
(a) Dry fiber
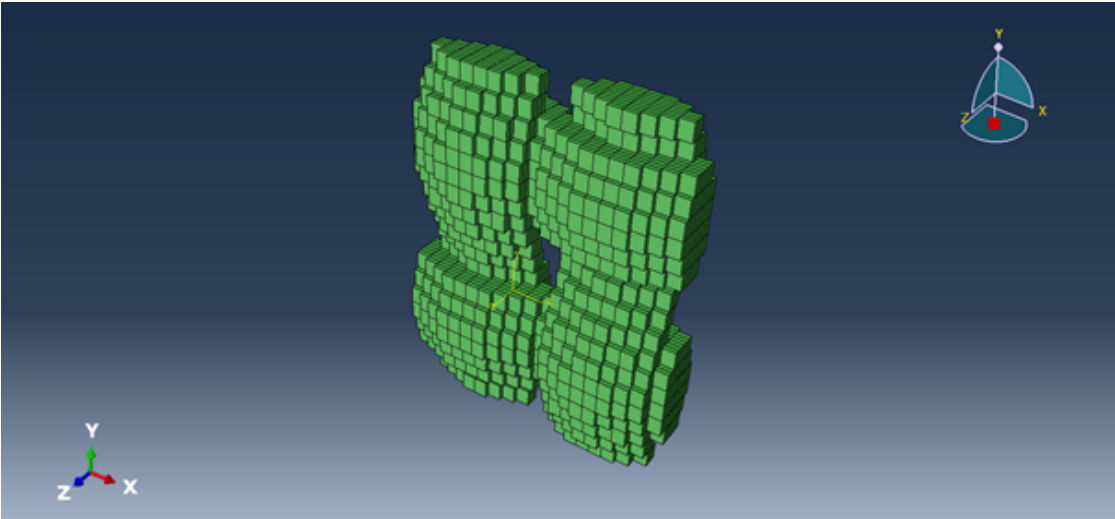
(b) Voxel

Figure 10: Plain weaves exported as dry fiber and as voxel file

The modelled yarn can be exported as a variety of different files. Important for this research are the dry fiber file and the voxel file. The dry fiber file is a file only containing the fiber. It is shown in Figure 10a. The surface of this file is smooth and friction between the yarns is modelled. The voxel file is made up of cuboids. It is exported with a matrix material surrounding the fibers. In Figure 10b the matrix is removed in order to make the yarns visible. Each of the cuboid in

the fiber-matrix block is calculated to have either the properties of the yarn or the matrix depending on where the middle point of the element lays. The voxel file can be exported with different amounts of cuboids in each direction. The more cuboids are being used, the more precise is the calculation. Too many cuboids on the other hand are computational very expensive and take a long time to compute for little to no gain in precision. In Figure 10b 50 cuboids are used in each direction. The resulting structure is not as smooth as the dry fiber file and does not offer the ability to account for friction between the yarns. Nonetheless the voxel file is an important tool to investigate the resulting properties due to its ease to handle. In both cases three files are exported. The element information and information about the orientations of the yarns are stored in the .eld or .ori file respectively. The .inp file is a standard Abaqus input file which stores the coordinates of the elements, which element to use, material parameters, boundary conditions and loads.

2.7 Homogenization

Homogenisation of the elastic stiffness properties is a common approach to design composite structures [10]. It is a widely used tool to obtain the overall properties of composites by applying a prescribed load to a volume. From which the mechanical response the material properties can be deduced [17]. If an linear elastic material is investigated where perfectly periodic boundary conditions can be applied the estimate obtained from the periodic homogenisation can be exact [18].

The composite is partitioned in representative volume elements (RVE). Representative volume elements are the smallest volume in a composite which captures the overall behavior of the composite. It is assumed to be part of a periodic material. A repetition of the RVE should result in sufficient accuracy of representing

the macroscopic appearance of the materials. The RVE should be selected in a way that the micro structure is composed of copies of the in full detail modeled RVE. Gaps or overlapping between boundaries should be avoided. On the one hand, a RVE has to be sufficiently small to neglect the influence of macroscopic properties. On the other hand, it has to be large enough to allow for meaningful sampling of micro scale stress and strain fields. The size and shape of an RVE depends on the parameters to be investigated. A RVE for mechanical investigations might look different than one for thermal ones [17, 10, 18]. Figure 11 shows periodic RVEs before and after loading. It can be seen that these RVEs are detailed enough to represent the whole fabrics micro structure. After the modeling of the RVE

RVE

RVE under loading

Unstressed structure of composite material

Periodic RVEs build-up

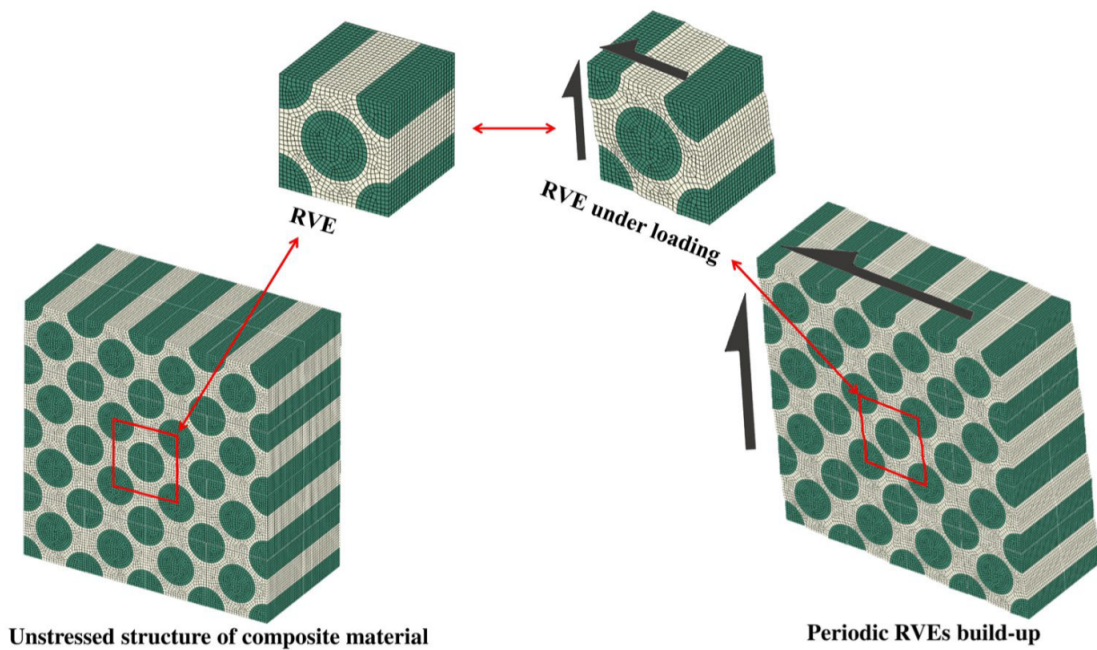Figure 11: Illustration of periodic RVEs build up before and after loading [10]

different loading conditions are applied and the response of the RVE is recorded. Most of the times the loading conditions are simple loads like uniaxial stresses [18]. From material response the macrostress and macrostrain are derived by averaging the stress and strain tensors over the volume of the RVE. The averaging equations

are shown in equations 23 and 24.

$$\overline{\sigma_{ij}} = \frac{1}{V_{RVE}} \int_V \sigma_{ij}(x, y, z,)dV \tag{23}$$

$$\overline{\varepsilon_{ij}} = \frac{1}{V_{RVE}} \int_V \varepsilon_{ij}(x, y, z,)dV \tag{24}$$

The RVE is then modeled as a homogeneous orthotropic material with the effective properties calculated. It describes the average material properties of the composite. With the homogenization method, material properties such as the Young's modulus, Poisson's ratio and transverse moduli can be obtained. [10]

2.7.1 Periodic Boundary Conditions (PBC)

Since a single unit cell or RVE is not enough to represent the whole fabric the adjacent cells have to taken into account [1]. This can be done with periodic boundary conditions. Periodic boundary conditions (PBC) are linking two opposite sites of the fabric together, so that one site moves, the other has to move with it. Essentially this is the same as calculating an infinitely large fabric. The PBC has two conditions which must be satisfied: The displacement must be continuous and neighbouring unit cells or RVEs cannot overlap or be separated [17].

In this thesis, the nodes of the opposing site are linked together by equations. This is called node-to-node periodic boundary conditions. These equations differ depending on a elastic or a shear modulus is investigated. In the following the equations for the calculations of the elastic modulus E_{11} are discussed as an example. For a detailed discussion of each load case, the reader is referred to Omairey et al. [10].

Given a cubic RVE to investigate E_{11}, a displacement in 1-direction has to be assigned. This displacement can only be assigned in the surface pointing in the 1- or -1-direction. Thus the nodes on these two opposing surfaces have to stay an
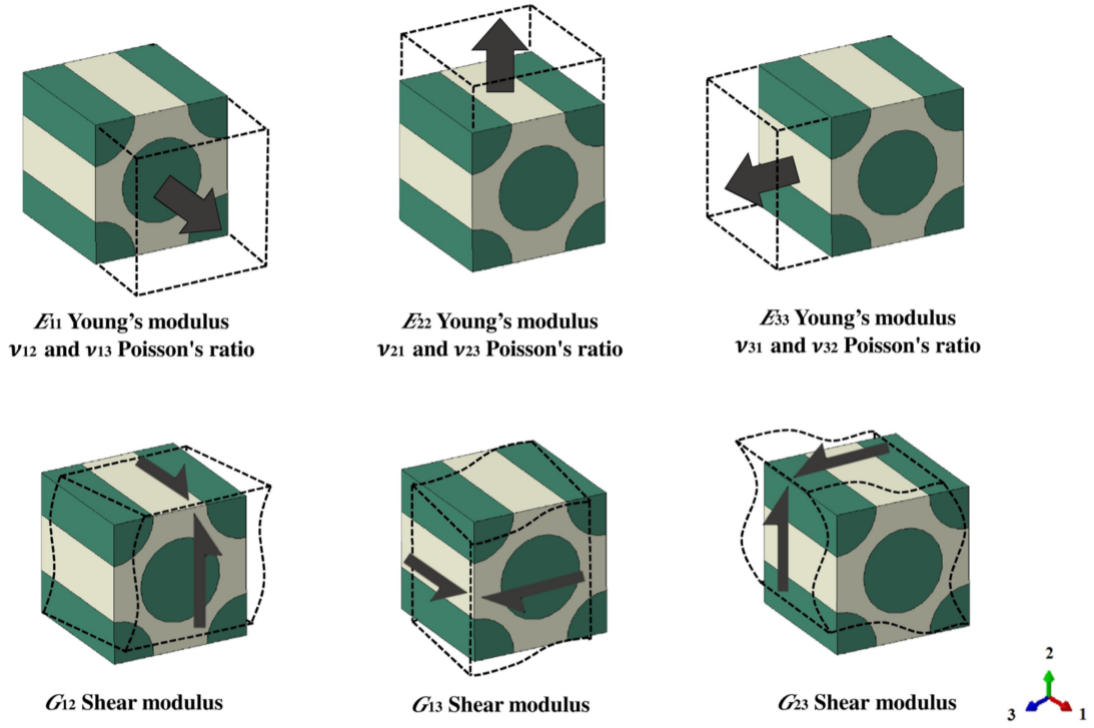
Figure 12: Schematic representation of displacement BC required to estimate effective elastic properties [10]

assigned values apart. In the 2- and 3-direction these nodes cannot move relative to each other since the PBC have to simulate a neighbouring RVE pulling with equal force on in the 2- and 3-direction. This is also the reason why the surfaces facing in the 2-, -2-, 3- and -3-direction cannot change their distance relative to each other in any spacial direction. The following equations show these conditions mathematically where X, Y, Z are the 1-, 2- and 3-directions respectively, the front and Back surface are facing in 1- and -1-direction, Top and Bottom in 2- and -2-direction and Left and Right in 3- and -3-direction [10] .

$$X_{Front} - X_{Back} = \text{Assigned value} \tag{25}$$

$$X_{Top,Left} - X_{Bottom,Right} = 0 \tag{26}$$

$$Y_{Front,Top,Left} - Y_{Back,Bottom,Right} = 0 \tag{27}$$

$$Z_{Front,Top,Left} - Z_{Back,Bottom,Right} = 0 \qquad (28)$$

List of References

[1] R. Misra, A. Dixit, and H. S. Mali, "Finite element (fe) shear modeling of woven fabric textile composite," *Procedia materials science*, vol. 6, pp. 1344–1350, 2014.

[2] A. R. Horrocks and S. C. Anand, *Handbook of technical textiles*. Elsevier, 2000.

[3] C. Cherif *et al.*, *Textile Werkstoffe für den Leichtbau*. Springer, 2011.

[4] P. Beccarelli, *Biaxial testing for fabrics and foils: Optimizing devices and procedures*. Springer, 2015.

[5] N. McCormick and J. Lord, "Digital image correlation," *Materials today*, vol. 13, no. 12, pp. 52–54, 2010.

[6] S. Yoneyama and G. Murasawa, "Digital image correlation," *Experimental mechanics*, vol. 207, 2009.

[7] T. Chu, W. Ranson, and M. A. Sutton, "Applications of digital-image-correlation techniques to experimental mechanics," *Experimental mechanics*, vol. 25, no. 3, pp. 232–244, 1985.

[8] H. Altenbach, *Kontinuumsmechanik*. Springer, 2012.

[9] M. H. Sadd, *Elasticity: theory, applications, and numerics*. Academic Press, 2009.

[10] S. L. Omairey, P. D. Dunning, and S. Sriramula, "Development of an abaqus plugin tool for periodic rve homogenisation," *Engineering with Computers*, vol. 35, no. 2, pp. 567–577, 2019.

[11] M. Bäker, "Numerische methoden in der materialwissenschaft," 2009.

[12] D. L. Logan, *A first course in the finite element method*. Cengage Learning, 2016.

[13] Abaqus/Simulink. "Abaqus documentation." July 2021. [Online]. Available: https://abaqus-docs.mit.edu/2017/English/SIMACAEEXCRefMap/simaexc-c-docproc.htme

[14] S. T. Peters, *Composite filament winding*. ASM International, 2011.

[15] University of Nottingham. "Texgen." June 2021. [Online]. Available: http://texgen.sourceforge.net/index.php/Main_Page

[16] M. Sherburn, "Geometric and mechanical modelling of textiles," Ph.D. dissertation, University of Nottingham Nottingham, UK, 2007.

[17] F. Ye and H. Wang, "A simple python code for computing effective properties of 2d and 3d representative volume element under periodic boundary conditions," *arXiv preprint arXiv:1703.03930*, 2017.

[18] M. Shahzamanian, T. Tadepalli, A. Rajendran, W. D. Hodo, R. Mohan, R. Valisetty, P. Chung, and J. Ramsey, "Representative volume element based modeling of cementitious materials," *Journal of engineering materials and technology*, vol. 136, no. 1, 2014.

CHAPTER 3

Modelling of the fabric

This chapter will present the two models developed in this thesis. As a first approximation, a netting analysis was implemented. The second model is a three dimensional Finite Element model, which is divided into a voxel and a dry fiber model.

3.1 Netting Analysis

To get a first quick estimation of the fabric material properties a netting analysis was conducted. It is assumed that only the yarns carries axial load. The weaving of the fibers is hereby neglected. The yarns go straight without interacting with one another or with the matrix around them. A visualization of the geometric assumption is depicted in Figure 13. A load applied to one of the
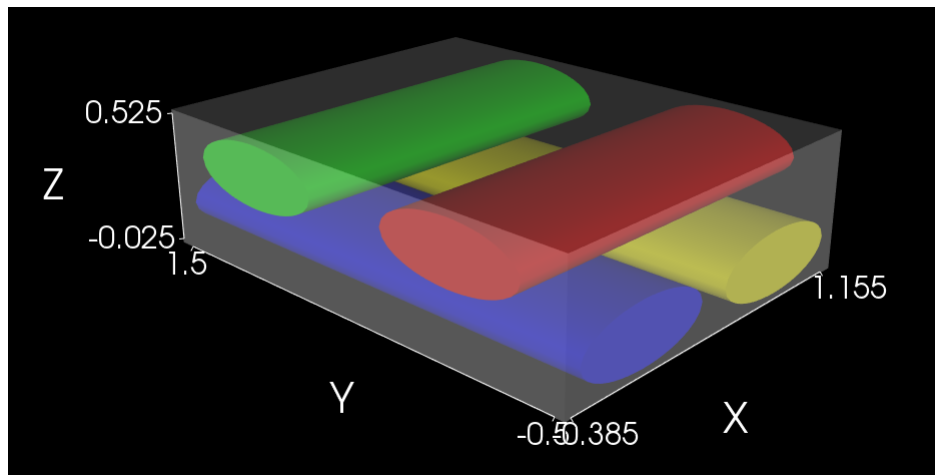

Figure 13: Geometric assumptions of the netting analysis

side faces is assumed to be carried by the yarns normal to that face. Since the composite material is made up of a yarn and the void between the yarns, the load can also be described by the modulus of the yarn and void with their respective

areas. This results in equation 29.

$$E_{eff} \cdot t \cdot d = E_{yarn} \cdot A_{yarn} + E_{void} \cdot A_{void} \qquad (29)$$

Since $E_{void} = 0$ the equation reduces to:

$$E_{eff} \cdot t \cdot d = E_{yarn} \cdot A_{yarn} \qquad (30)$$

Rearranging gives:

$$E_{eff} = E_{yarn} \cdot \frac{A_{yarn}}{t \cdot d} \qquad (31)$$

With a measured value of 0.99 GPa for the yarns modulus, as discussed in chapter 4.3, the cross sectional area of one yarn estimated as 0.1247 mm^2 and the dimensions of the surrounding void in the unit cell as 1.54 mm x 2.00 mm x 0.55 mm the effective material properties are

$$(E_{eff})_{weft} = 220 \text{ MPa and } (E_{eff})_{warp} = 290 \text{ MPa}$$

3.2 Development of a Finite Element Model

In order to run a three dimensional simulation of the woven fabric using Tex-Gen and Abaqus to examine its behaviour several steps are required. The individual steps, which can be seen in Figure 14 are discussed below. The first two steps in dark blue are discussed in Chapter 4.3 where the linear elastic properties of the yarn material were investigated. Since the transverse and shear moduli as well as the Poisson's ratio of the yarn are not measureable with the setup in the laboratory, they need to be estimated. This will be discussed further in section 3.2.2. Two different modeling approaches will be discussed in this section. The TexGen generated voxel file is analysed in Abaqus using EasyPBC, an Abaqus plug-in designed by Omairey et al. [2] to determine the linear response of the material. This model provides the linear elastic properties of the fabric. The TexGen
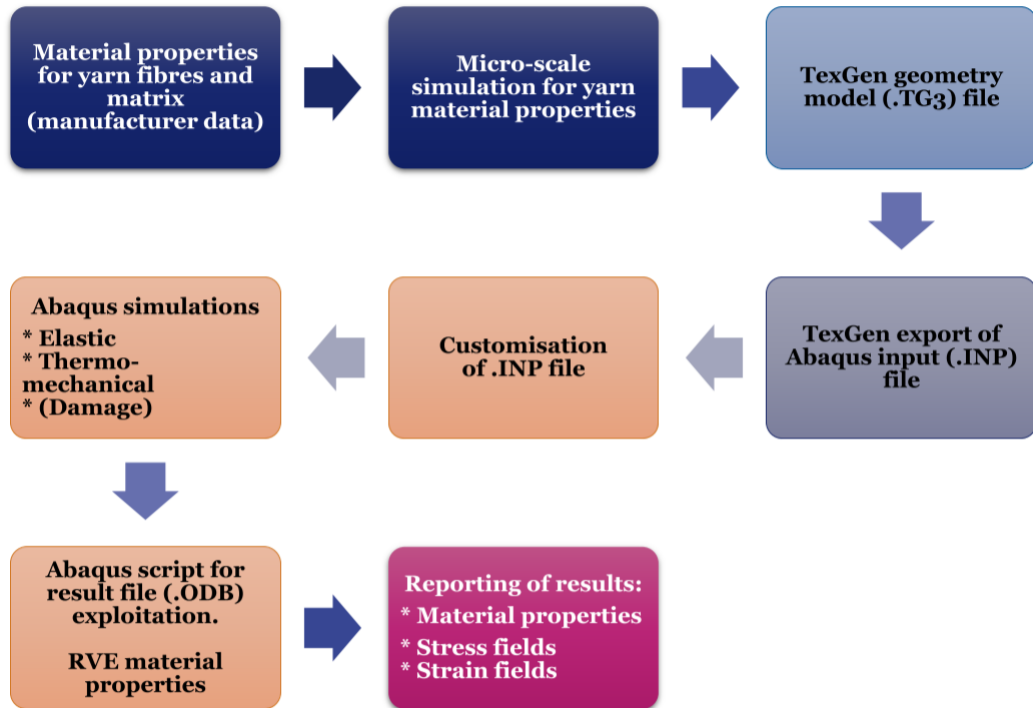
Figure 14: Workflow with the TexGen program[1]

generated dry fiber file models the fabric in greater detail and includes effects of friction and yarn decrimping. These elements determine the nonlinear response of the fabric.

3.2.1 Geometric Modelling

The fabrics geometry was modeled with TexGen. In order to produce an accurate model in TexGen the measured geometric data needs to be inserted into the program. TexGen can develop an accurate geometry using only six inputs. The geometrical data are shown in Table 2. Since the default cross section of TexGen is very close to the actual cross section of the fabric as seen under a microscope, the default cross section was selected in the model. Both cross sections can be seen next to each other in Figure 15.

The geometric input data need to be input in the dialog box, the weave wizard, which opens once the plain weave option is selected. In the weave wizard, the

(a) Microscopic picture   (b) Texgen picture

Figure 15: Side view of the fabric

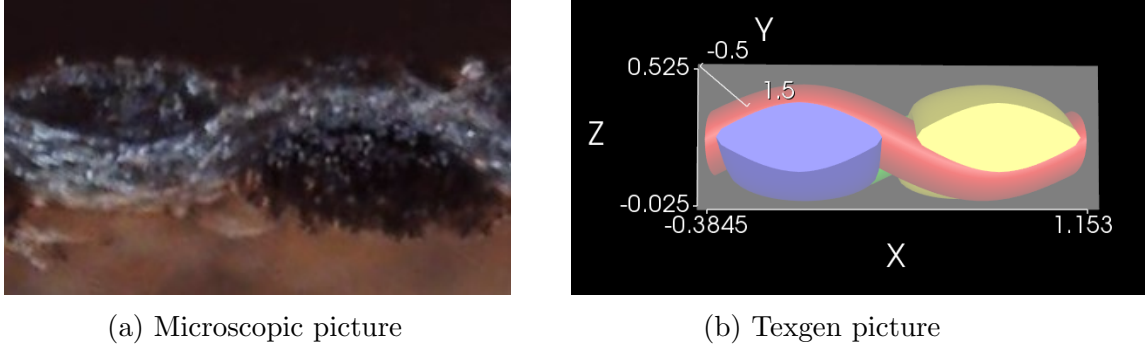geometry of the fabric is specified. It gives a variety of options. The first to select is the amount of yarns in warp and weft direction. For the 1000 denier fabric two yarns in each direction are chosen to define the unit cell.

The next thing to be input are the geometric properties of the yarn, the yarn width, the fabric thickness and the yarn spacing. To calculate the yarn spacing one just has to invert the number of yarns per centimeter to get the spacing in centimeters. These can then easily be transferred to every other unit. The fabric has different spacing in both directions, thus the average spacing can be entered. The yarn width and fabric thickness are the same in both directions, so the measured value can be entered. The remaining check boxes can stay in the default setting. The created domain is a box surrounding the unit cell. It is important for the use of the EasyPBC plugin need to be modelled and exported. The model should also be refined since that option prohibits the yarns from intersecting into one another. With this option ticked, the model always contains a gap size between the yarns. This gap size can be zero to create contact and friction. If a shear model is needed, shear can be applied to the model in a arbitrary angle which can be specified. In the given case no shear is applied.

The next step is to determine the weave pattern. With only two yarns in each direction this step is fairly straight forward. After selecting the next option in the

weave wizard a windows opens in which the pattern can be specified. To lay one
yarn above another one the respective intersection is selected with a left mouse
click. The second adjustment to be done in this window is the individual yarn
setting for each direction. To select all yarns in one direction the boxes on the
edge of the yarns can be selected by shift click, with a right click the yarn spacing,
height and width can be set. In the case presented in this theses, the yarn spacing
in warp and weft is different.
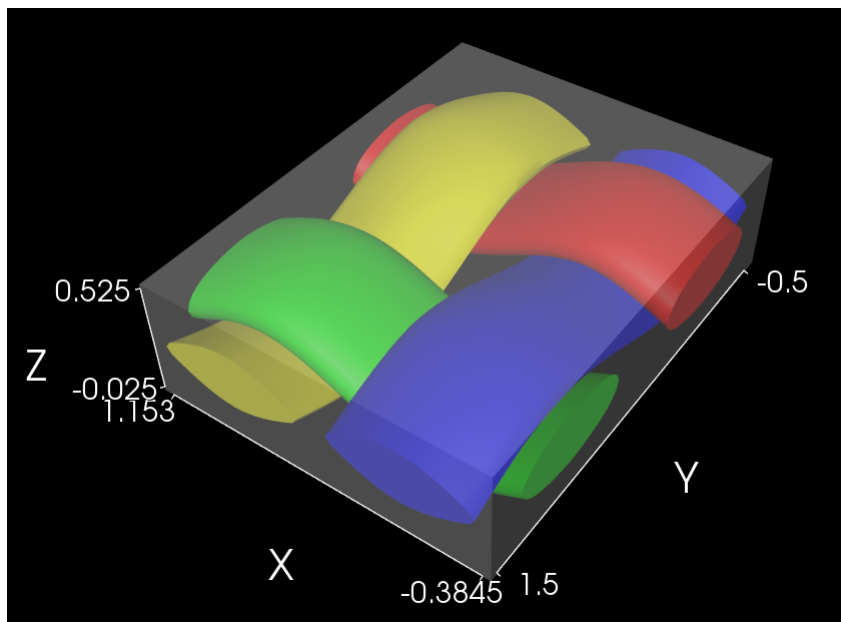
Figure 16: Screenshot of the geometry design in TexGen

After confirming the entries, TexGen models the geometry. For fabrics with a
different cross section, the cross section can be adjusted in the modeller tab under
assign section. There the different cross sections as discussed in section 2.6 can
be implemented. The finished design of the unit cell of the examined fabric is
shown in Figure 16. The warp direction has more fibers per unit length than the
weft direction. This difference in accounted for with a rectangular unit cell which,
when repeated, will result in the same fibers per length as the real fabric in each
direction.

36

The finished geometry can then be exported in different ways. Important for this thesis are the voxel and dry file discussed in the following sections.

3.2.2 Voxel Model

Figure 17: Voxel geometry opened in Abaqus

Once a voxel file is exported, TexGen creates three files. The element data is stored in the .eld file and the data about the element orientation is stored in the .ori file. Neithe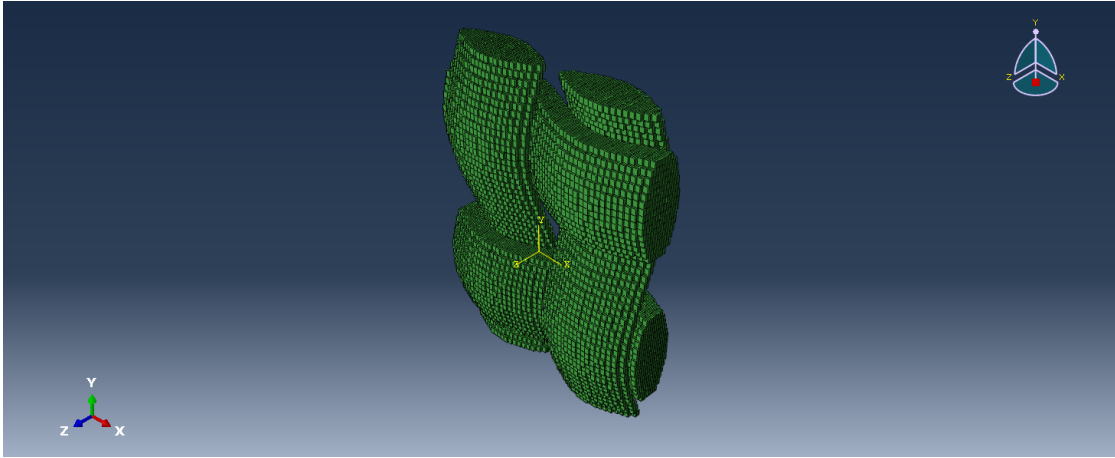r of these files need to be edited for simulations to run. The third file, the input file, contains a script which Abaqus can interpret as a model. The contents of this file are shown in Figure 18. The input file can be structured in seven different segments. At first the mesh is defined. The coordinates of each nodes are defined. The second step is the element definition where the different types described in section 2.4.2 are assigned to the elements. In the voxel model an eight node brick element is used with (C3D8R) or without (C3D8) reduced integration and hourglass control. The orientation and coordinate system of the yarn is defined in the next step. After the definition of the orientation, element sets and node sets are created. The different sets are important to distinguish the yarns from the matrix and from one another. The last two steps are the definition of the periodic boundary conditions as well as the step definition with output request.
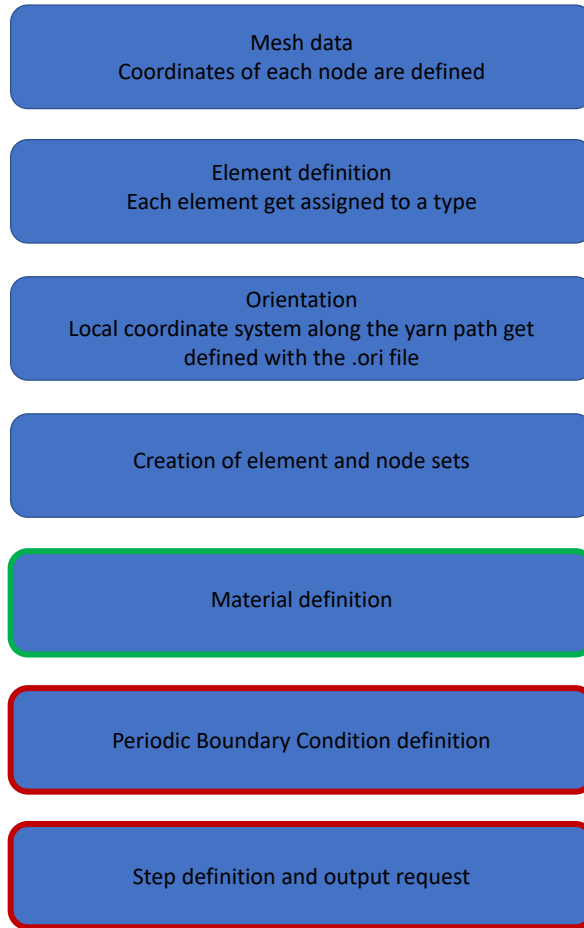
Figure 18: General structure of the voxel input file. Some code segments have to be edited (green) some have to be deleted (red)

This input file needs to be edited in order to perform the simulations. The last steps, indicated by a red rim can be deleted since the EasyPBC plugin defines periodic boundary conditions and the equations generated by TexGen are not needed. The steps are also replaced by EasyPBC.

The material definitions in step 5 have to be edited to match the yarn and matrix material as closely as possible to get accurate simulation results. For the matrix an extremely low Young's modulus $E_1 = 1$ Pa and a Poisson's ratio $\nu = 0.3$ are chosen. The real fabric is not embedded in a matrix, but since the EasyPBC plugin needs to have a matrix to determine the material properties correctly, it

cannot be simply deleted. The yarns are assigned the Young's modulus measured in chapter 4.3. Since it was not possible to measure the transverse and shear moduli as well as the Poisson's ratio of the yarns these need to be estimated. This procedure will be discussed in chapter 4.

After these changes the model is loaded into Abaqus CAE. Subsequently the EasyPBC plugin can be started. The plugin then defines specific load cases that are used to calculates the linear elastic material properties of the fabric and saves the results in a text file.

Voxel refinement
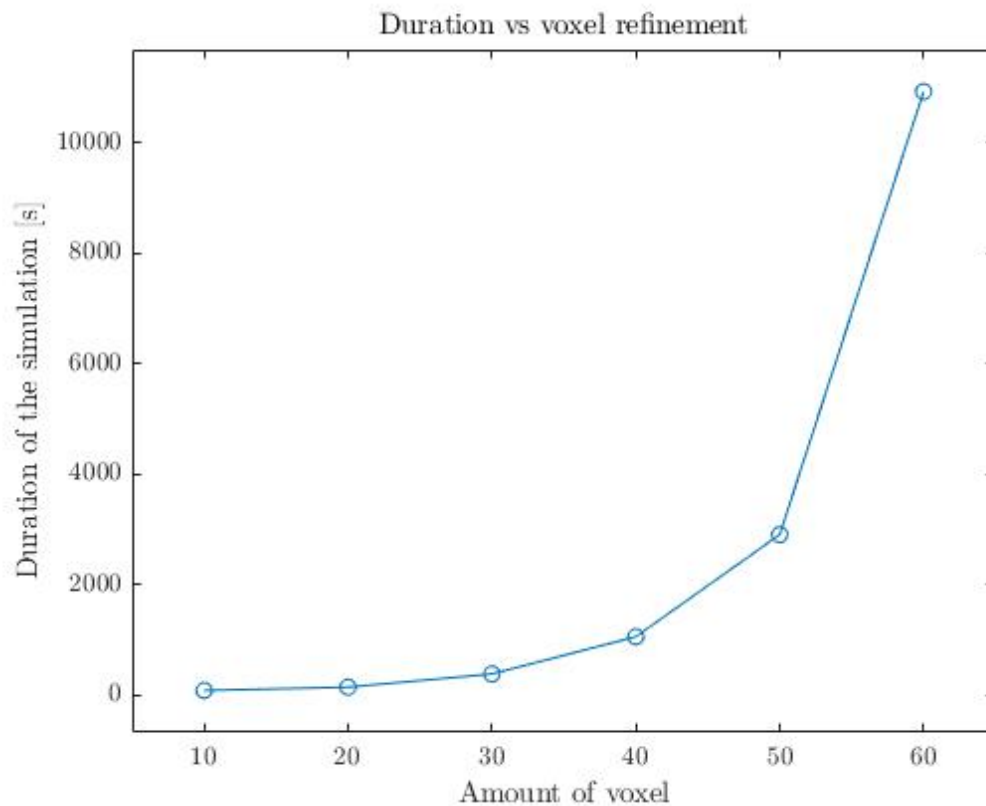
Figure 19: Duration of the voxel simulation vs voxel refinement

The first step in conducting a voxel analysis is deciding how refined the voxel model needs to be. Since a voxel model is made out of cuboids, generally speaking

the more cuboids an analysis has, the more precisely it can predict the actual material behavior. The computational cost rises as the more cuboids are used. To determine a good compromise between accuracy and computational expense, a study was conducted with models of varying voxel refinement. Six different models were chosen, the smallest one contains 10x10x10 cuboids, the largest one 60x60x60 cuboids. Figure 20 shows the duration of the simulation as a function of the number of voxels in the model. From the graph can it can be seen that the calculation time increases dramatically when the number of voxel used is increased. While the first simulation took roughly one minute, the largest simulation ran for over three hours.

Figure 20: Young's modulus in weft direction vs voxel refinement

Figure 20 shows the predicted Young's modulus in weft direction for each of the voxel cases. While all of the simulated moduli are of the same order of

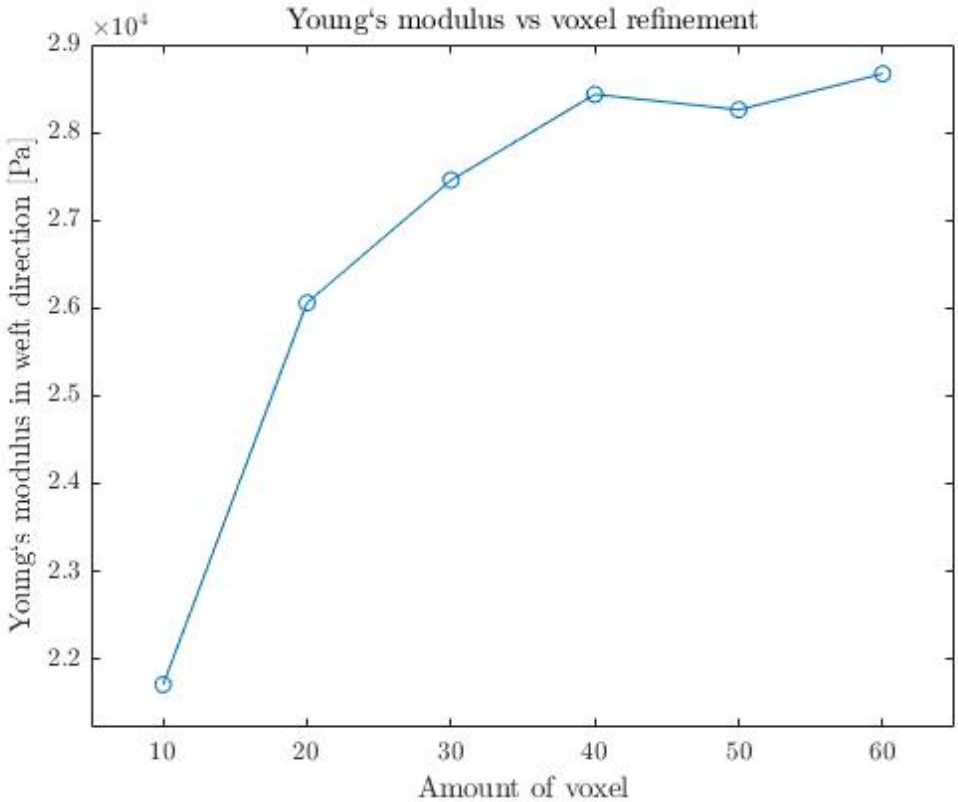magnitude, the results are significantly lower in the models with fewer cuboids. The value for Young's modulus appears to converge for cases with 40x40x40 and higher cuboids. Between the 40x40x40 and 60x60x60 voxel mesh Young's modulus differs by only 0.8%.

Hence the 40x40x40 voxel mesh was selected for the remaining simulations since it offers good accuracy and small computational costs.

3.2.3 Dry Fiber Model
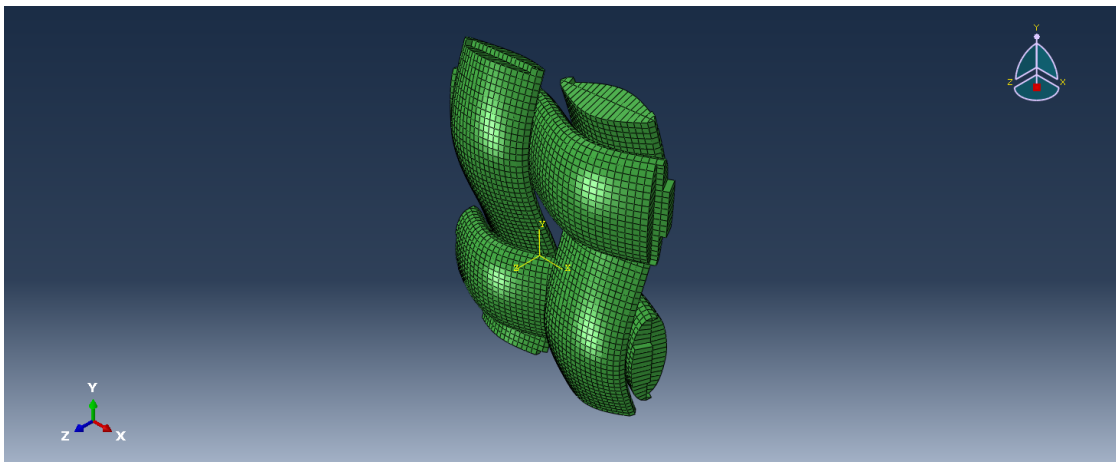
Figure 21: Dry fiber geometry opened in Abaqus

Similar to the voxel file, TexGen creates three output files while exporting the dry fiber file. All files have the same purpose as with the voxel file. The input file also looks similar to the input file of the voxel file with a few additional steps. The general steps are shown in Figure 22. The first four steps are equivalent to the first four steps in the voxel input file. But since the dry fiber file can be exported without a matrix, there is no need for the creation of a matrix element set. Nonetheless different types of set are created. Notably all the nodes on the cross section of the yarn are collected in four sets: Front (Bound0A), Back (Bound0B), Left (Bound1A) and Right (Bound2B). The material of the yarns still have to be inserted to match the yarn properties as closely as possible. The next step is the
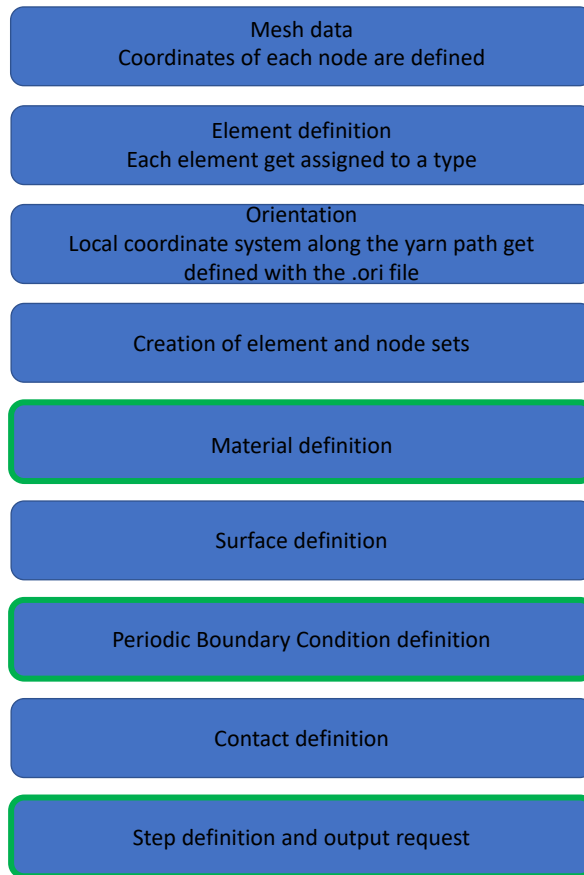
Figure 22: General structure of the dry fiber input file. Some code segments have to be edited (green) some have to be deleted (red)

definition of surfaces. Since the dry fiber file can model friction, the surfaces where friction can occur needs to be specified. The contact definition have to be specified for the same reason.

The periodic boundary conditions have to be edited to account for adjacent unit cells. The boundary conditions work with the same system as discussed in section 2.7.1. But instead of an assigned value a dummy node is inserted into the equations where the respective cross sections of the yarns are facing. The edited

equations are:

$$X_{Bound0A} - X_{Bound0B} - X_{Dummy0} = 0 \tag{32}$$

$$Y_{Bound1A} - Y_{Bound1B} - Y_{Dummy1} = 0 \tag{33}$$

Additional to editing the equation, the movement in the Z-direction cannot be prohibited by boundary conditions or equations since the fabric has to be allowed to contract in this direction when pulled.

The dummy nodes are nodes which are located at the origin. They are not part of the original model but separated and only connected to the model by the periodic boundary condition equations. These nodes can be displaced to assign a value to the equations as in Equation 25. This allows for periodic boundary condition as well as for the possibility to have different steps with different load cases. The dummy nodes can for example be displaced in X- or Y-direction respectively in the first step to create biaxial tension. In the second step only one of the nodes can be displaced even further to introduce a more complex stress case.

To prevent solid body displacement, one node has to be held in place by a boundary condition. The node chosen lays in the geometric center of one of the yarn to introduce as less stress as possible with this boundary condition.

The dry fiber model can, in contrast to the voxel model, portray non linearities such as geometric non linearities and friction.

Depending on the simulation, the step definition has to be changed. For complex fabric behaviour, several load increments may be necessary. For the evaluation of the simulation the element volume has to be specified as an output. The evaluation will be discussed in chapter 4.

Before the dry fiber model can be used to predict material behavior, accurate yarn properties have to be determined. Once the yarn properties are entered in the

input file, the load case to be investigated is determined, and the step definition adjusted accordingly, Abaqus can run the simulation. The TexGen generated input file cannot be started in Abaqus CAE but has to be initiated by the command window. The command window has to be opened in the directory where the input, .eld and .ori file are located. The job can then be started by the command

$$\texttt{abaqus job =} \textit{ input-file-name.}$$

Note that the model's periodic boundary conditions are specified in the TexGen generated input file in a way Abaqus CAE cannot execute.
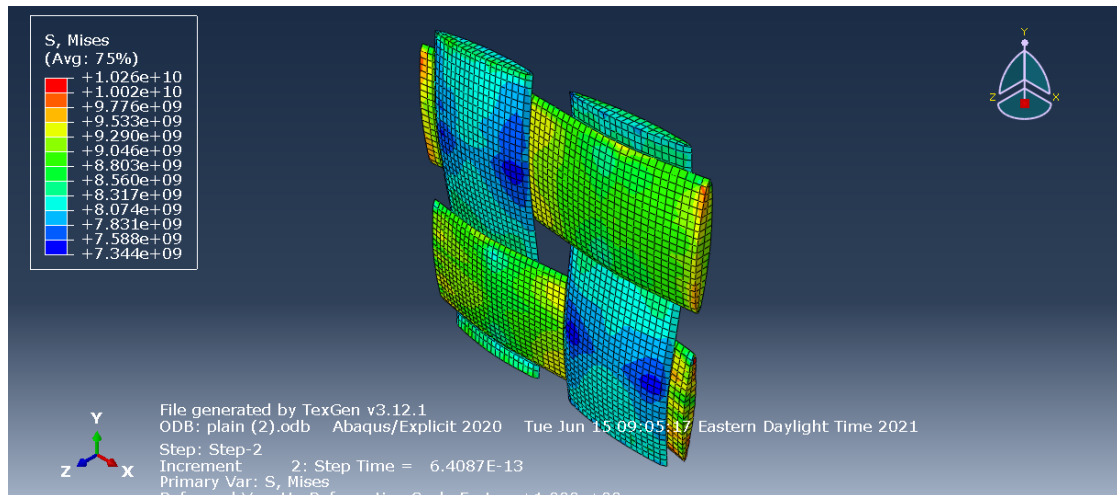
Figure 23: Simulation result as it can be seen in the .odb file

Once the simulation is finished, the results can be examined in the .odb file generated by Abaqus. A typical a result is shown in Figure 23. To plot the simulation data, a few steps have to be considered. The first step is to change the coordinate system from the local system which runs along the yarns to the global one. This can be done in Abaqus CAE by introducing a coordinate system manually which matches the global system and let Abaqus transform the stress and strain results to this global system. Then, in the .odb file the element volume (EVOL) as well as the stresses and strains calculated in each step are written to

an output file. That can be opened in Excel. These output files then can be edited for ease of input to a Matlab script used to plot the volume average stresses and strains over time. Typical plots are shown exemplary in Figure 24. Figure 24a shows the volume averaged stress in the global 1- or x-direction introduced by a load in the same direction. Figure 24b shows the volume averaged strain in the same direction introduced by the same load. Both plots can be combined into one

(a) Stress output over time   (b) Strain output over time
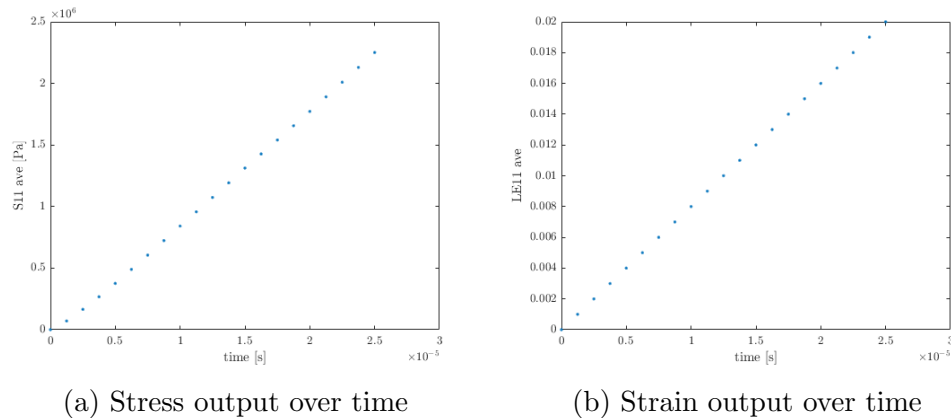
Figure 24: Results from the dry fiber simulation plotted over time.

plot to get a stress strain curve. Figure 25 shows the average stress over the whole unit cell versus the average strain. This curve can then be used to predict material properties of the woven fabric. Similar analyses can be performed to compute the modulus in the transverse direction as well as effective Poisson's ratios.

List of References

[1] University of Nottingham. "Texgen." June 2021. [Online]. Available: http://texgen.sourceforge.net/index.php/Main_Page

[2] S. L. Omairey, P. D. Dunning, and S. Sriramula, "Development of an abaqus plugin tool for periodic rve homogenisation," *Engineering with Computers*, vol. 35, no. 2, pp. 567–577, 2019.

Figure 25: Stress-strain curve determined by the dry fiber model with initial slope.

CHAPTER 4

Simulation Results

To investigate the behavior of the developed models, different studies are conducted. In the following chapter these studies are presented and the results presented. At the end of the chapter the different modelling approaches are compared with experimental results which are collected parallel to this thesis.

4.1 Yarn spacing

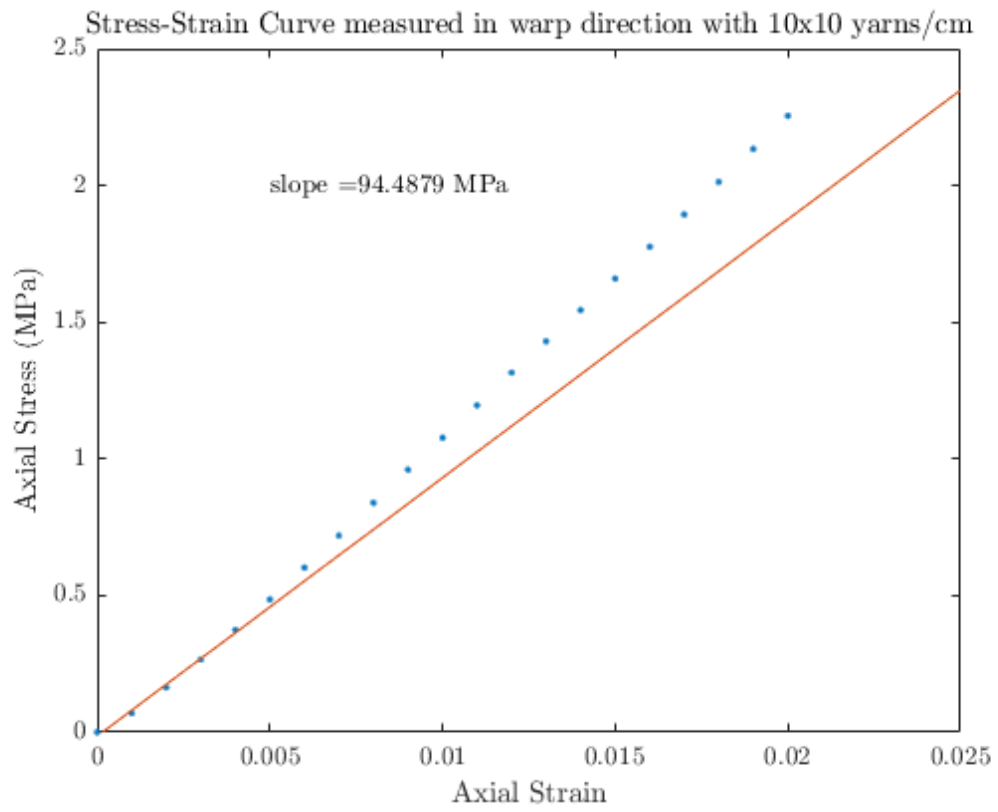The different modelling approaches and the influence of different yarn spacing are investigated in the first study. In the first step in conducting the study the geometric models are created and exported using TexGen. Four models with different spacing are being used. The base case has an equal spacing between the yarns in warp and weft direction. The yarn density of the base case is 10 yarns per centimeter. The number of yarns in weft direction used by the other models stays constant at 10 yarns per centimeter while the number of yarns in warp direction changes. The selected yarn densities are 12, 14 and 14.285 yarns per centimeter in warp direction. The closest the yarns could fit next to each other in the model are 14.285 yarns per centimeter, thus this number is chosen. The geometry of each fiber is modeled after the geometric measurements discussed in section 4.3. The yarn width is 0.635 mm and the yarn height is 0.25 mm.

The yarns Young's modulus is chosen to be 1 GPa based on the experimental data described in section 4.3. The transverse modulus is assumed to be 100 MPa, one tenth of the Young's modulus. The transverse modulus together with a generic Poisson's ratio of 0.3 give a shear modulus of 38.5 MPa through the equation

$$G = \frac{E}{2(1+\nu)}.$$

The void properties are chosen to be very low.

The results of the different simulations are shown in figures 26. All simulations are considering a uniaxial stress state with measurements in the same direction as the applied elongation. The blue curves are depicting Young's Modulus in the warp direction, where the yarn density changes, while the model is elongated in the same direction. The red curves are showing Young's Modulus in weft direction. Each of the three simulation methods have a different symbol assigned to them. The netting analysis has a '+', the voxel model a 'o' and the dry fiber model '*'.
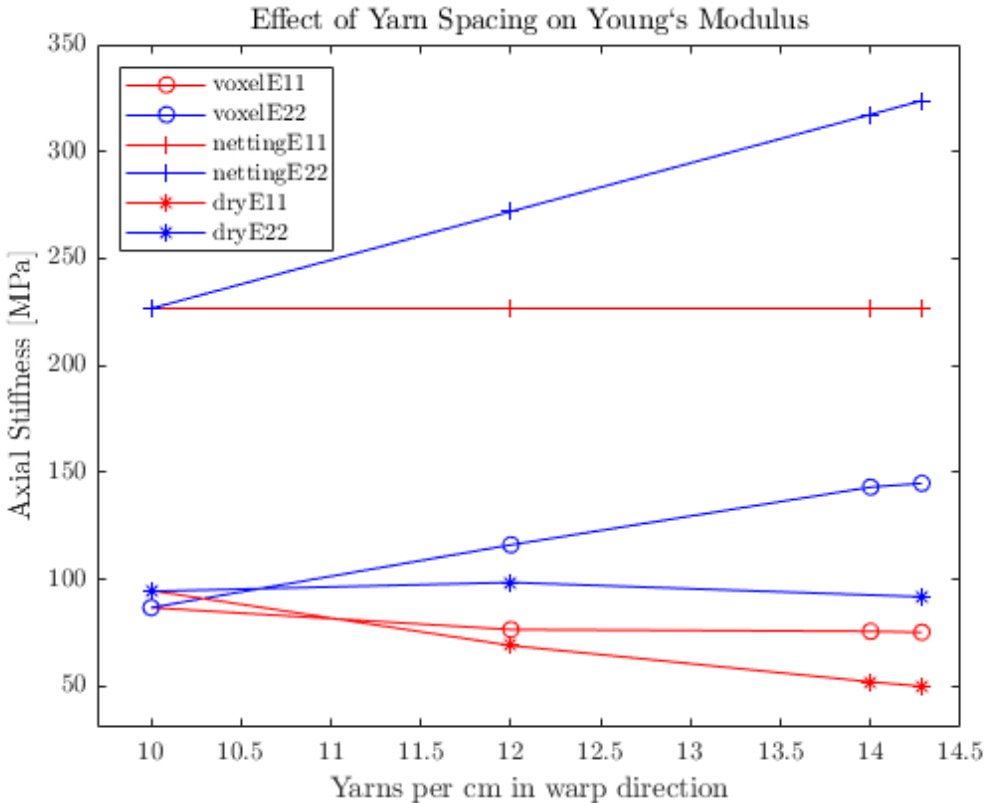

Figure 26: Comparison of the different modelling methods with different yarn spacings

The netting analysis is stiffer then both the voxel and dry fiber simulation. Netting analysis doesn't consider yarn interactions or crimping. The yarns are considered to lay straight and carry all the load with no interaction between the

yarns. In the weft direction, where the yarn spacing doesn't change, the resulting Young's modulus doesn't change either because of this lack of yarn interaction. In the warp direction, where the yarn density is increasing, Young's modulus increases linearly with yarn density. The voxel simulation shows a similar trend where the Young's modulus in weft direction only gets slightly lower with a higher yarn density. In the warp direction it almost also rises in a linear fashion. Since yarns are interacting in this kind of simulation some of the induced stress can be carried by the yarn running perpendicular to the measured direction, lowering the effective Young's modulus. This effect is even more present in the dry fiber simulations. The dry fiber and voxel results are very close to each other but the downwards
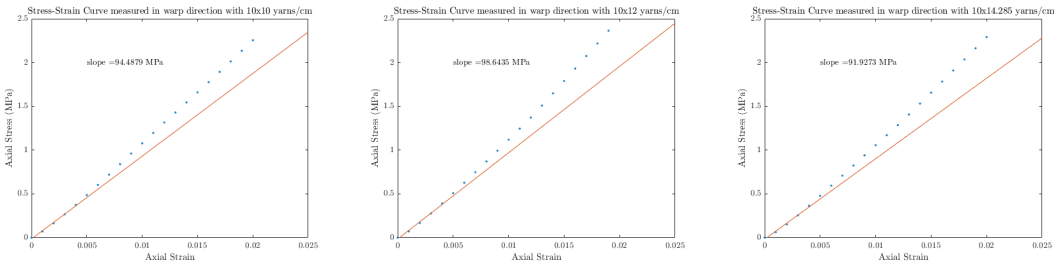
(a) 10 yarns/cm weft and warp

(b) 10 yarns/cm weft and 12 yarns/cm warp

(c) 10 yarns/cm weft and 14.285 yarns/cm warp

Figure 27: Stress-Strain curves in warp direction with different yarn spacings. The blue dots are the simulation results, the red line is a linear interpolation of the first five data points.

trend of the weft direction Young's modulus with increasing yarn density is higher than observed in the voxel model. In the warp direction the Young's modulus of the dry fiber simulation first increases slightly, then decreases with an increase of yarn density. This result is surprising, since more yarns in one direction means more yarns to carry load, thus a higher Young's modulus. In this curve, only three data points are present, since the simulation with 14 yarns/cm in warp direction exhibited hourglassing instability and inaccurate results. The 14.285 yarns/cm model used a different kind of element to prevent the hourglassing. This

numerical problem might explain the surprising results of this simulation and more investigation is recommended.

Figure 27 shows the stress strain curves generated by the dry fiber simulation. The blue dots are the data points calculated by Abaqus and subsequently averaged over the volume of the unit cell. The first five data points are then linear interpolated to get the initial slope. This initial slope is the initial stiffness modulus of the fabric. Figure 28 shows the results of the simulations calculating Young's modulus in weft direction.

(a) 10 yarns/cm weft and 10 yarns/cm warp

(b) 10 yarns/cm weft and 12 yarns/cm warp

(c) 10 yarns/cm weft and 14 yarns/cm warp

(d) 10 yarns/cm weft and 14.285 yarns/cm warp
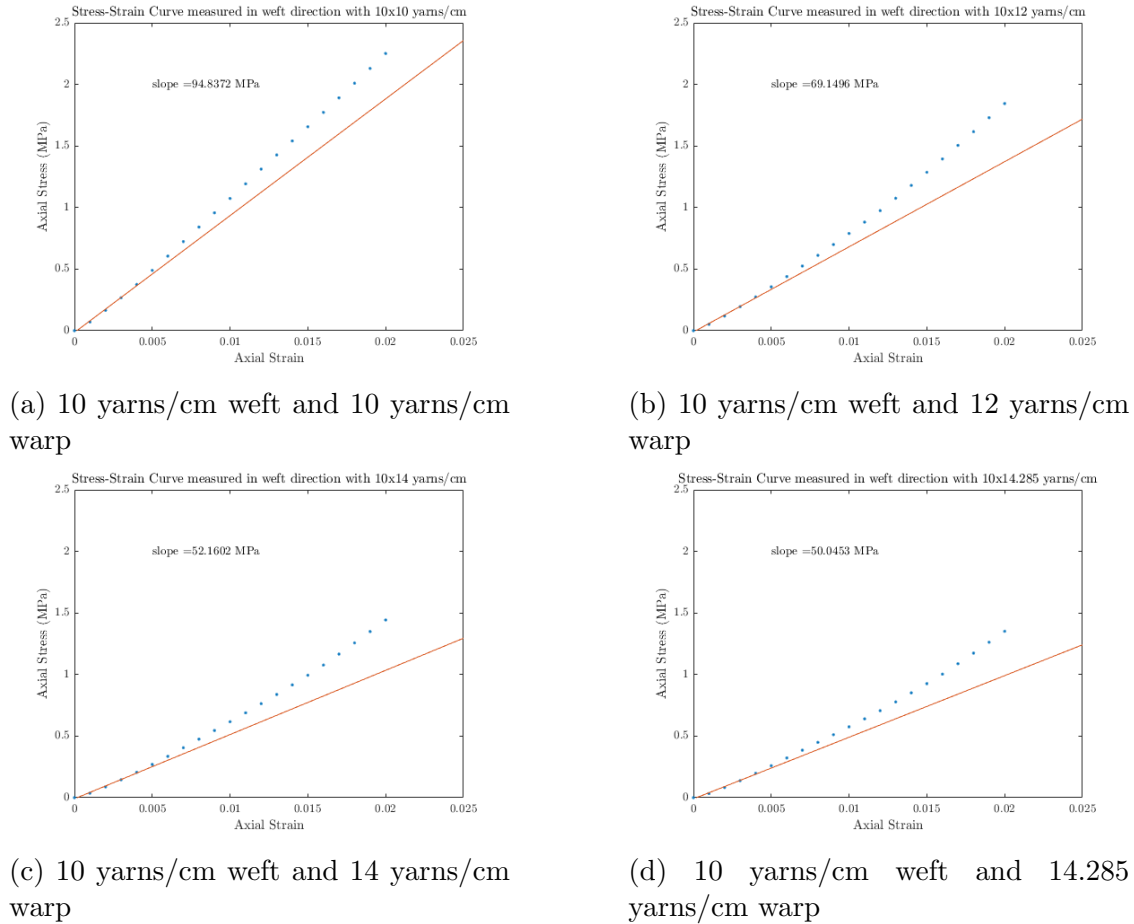
Figure 28: Stress-Strain curves in weft direction with different yarn spacings. The blue dots are the simulation results, the red line is a linear interpolation of the first five data points.

4.2   Biaxial Pre-strain

To investigate the effect of biaxial pre-strain another study was conducted. The motivation for this study was to simulate the behavior of inflated panels, which experience biaxial loading durin inflation followed by axial stressing during service. Since both the voxel and netting analyses are linear, pretension doesn't have an effect on these models, thus the dry fiber model is needed. As a model the base case with a yarn density of 10 yarns per centimeter in both warp and weft direction was used. The fiber geometry and elastic properties were kept the same as described in the previous section.
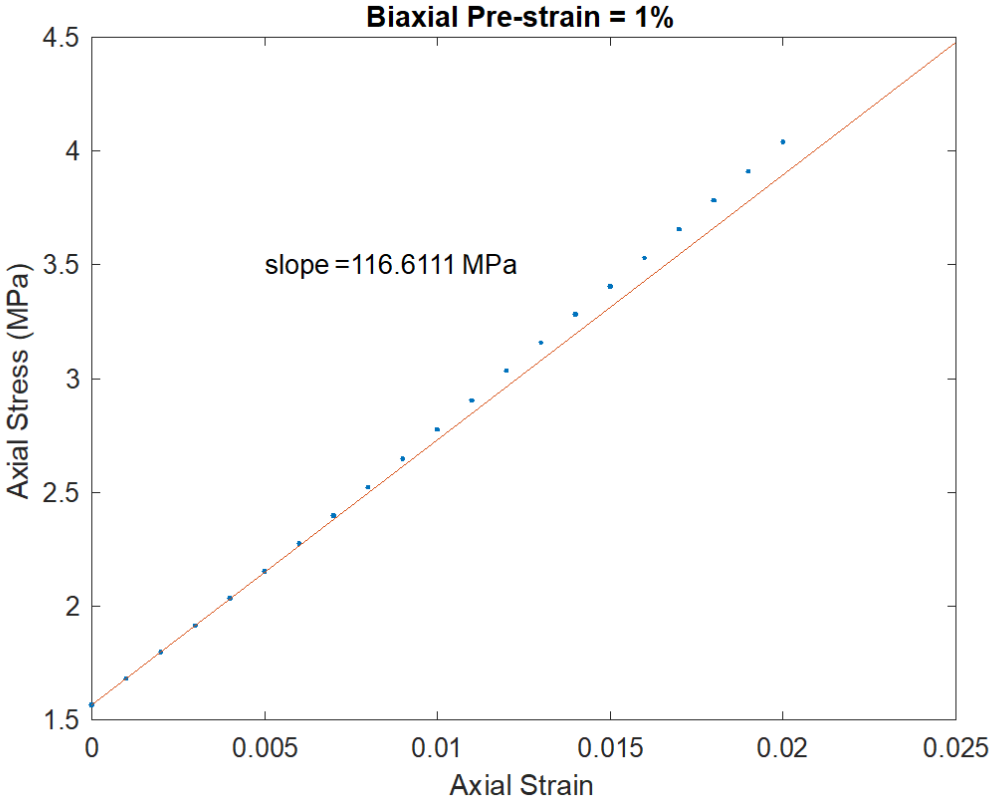
Figure 29: Stress strain curves of the second step after 1 % of Pre-strain.

The simulation consists of two steps. In the first step a biaxial pre-strain is applied. This biaxial pre-strain was varied between 1%, 2% and 3%. In the second step an additional strain of 2% was applied to the warp direction of the model.

The stress and strain of the second step were then extracted and averaged over the volume of the entire unit cell. These stress strain curves are shown in Figures 29, 30 and 31.
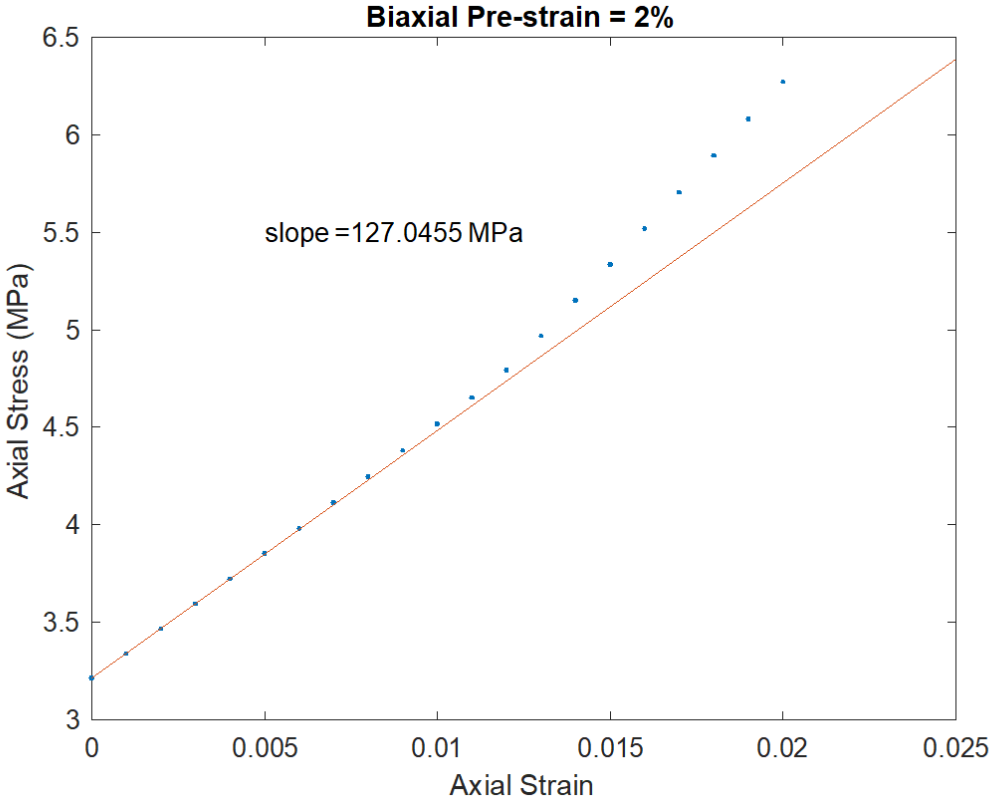
Figure 30: Stress strain curves of the second step after 2 % of Pre-strain.

The blue dots are the data extracted from Abaqus, the red line is a linear interpolation of the first five data points, the slope of which is the apparent Young's modulus. The apparent Young's modulus are summarized and plotted over the applied pre-strain in Figure 32 It can be seen that the model stiffens up with an increase in pre-strain. The exact correlation of this effect cannot be observed from only three data point. While more research is necessary, these results confirm experiment observation that under increased inflation pressure, woven fabric skins exhibit increased stiffness.
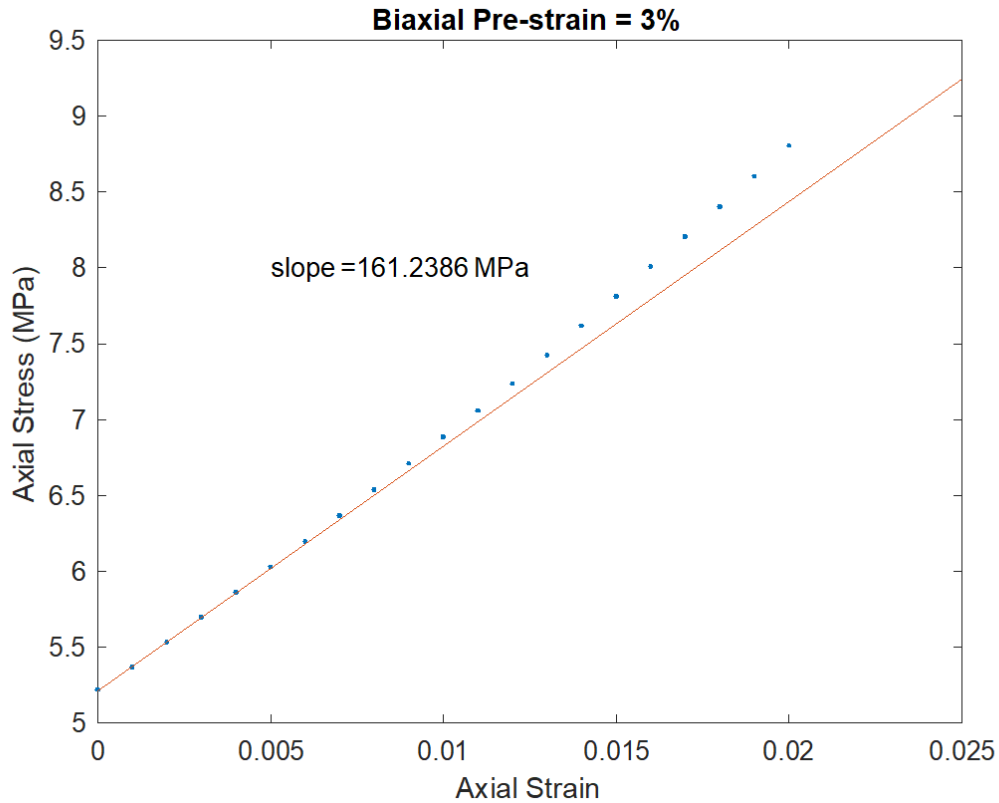
Figure 31: Stress strain curves of the second step after 3 % of Pre-strain.

4.3 Experimental Data

In this section, results of the parallel experiment study and the measurement of the geometry are discussed. Both the experimental data and the measurements were obtained by the students in Professor Taggart's research group. The fabric tested is a 1000 denier plain weave fabric with the individual yarns made out of nylon. Denier is a measurement of the linear mass density, defined as the mass in grams of a 9000 meter yarn length. Hence, a 1000 denier yarn has a mass of 1000 grams per 9000 meters. The weight of the woven fabric is 11.2 $\frac{oz}{yd^2}$.

4.3.1 Geometry Measurement

The geometrical structure of the fabric has a strong influence on the overall behavior. The model should represent this structure as closely as possible. In a
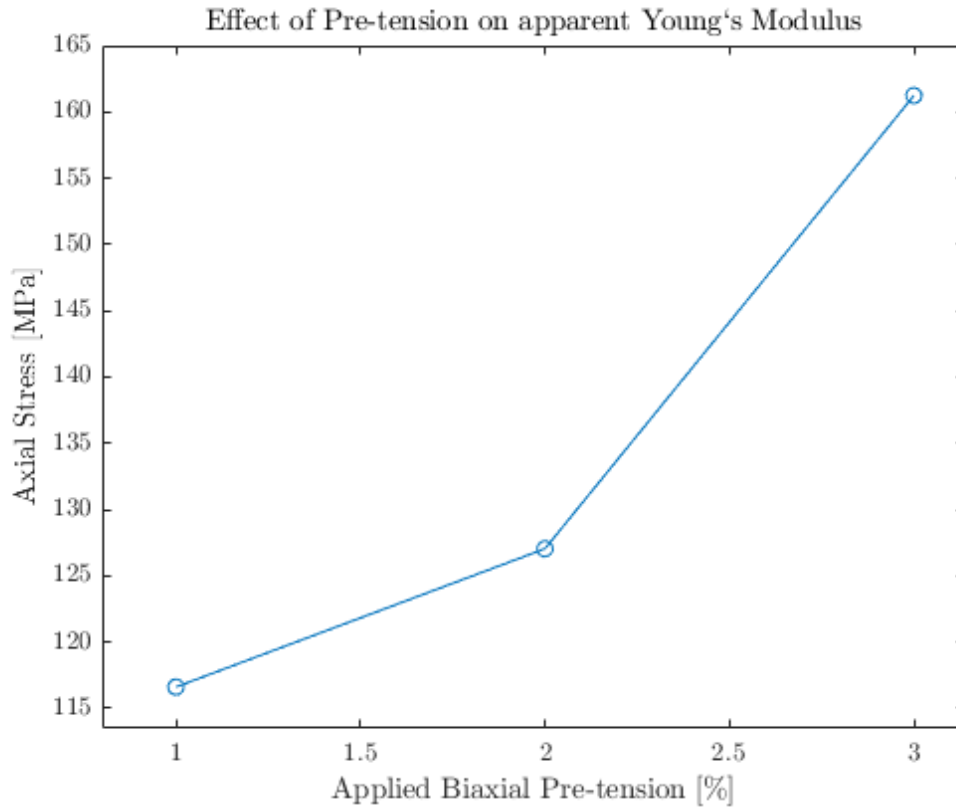
Figure 32: Duration of the voxel simulation vs voxel refinement

plain weave there are four measurements in each direction which can characterize a fabric. The first three measurements characterize the geometry of the yarn. The yarns cross section, the yarn width and the yarn height, all of which could change throughout the length of the yarn. It is assumed that each dimension remain constant in the tested fabric. Additionally the thread spacing in both the warp and weft directions is measured.

The measurements were taken with a special microscope that has an integrated micrometer. The micrometer allows for a precise movement of the table under the microscope which is also connected to the fabric sample and allows for alignment in order to measure the sample. With a fine line on the lens of the microscope a starting position is defined. The micrometer is then turned until the line on the lens reaches the end position. The traveled length can than be read off of the

Figure 33: Microscopic picture of the Denier 1000 fabric

micrometers vernier. A microscopic view of the fabric is shown in Figure 33. The red lines indicate the starting and end position of the measurement line on the microscope used to measure the yarns in plane dimensions. The yarn thickness is measured indirectly with a conventional micrometer by measuring the thickness of the fabric. The yarn thickness is taken to be half of the thickness of the fabric since at any point in the fabric these two yarns lay on top of each other. This can be seen in a side view of the fabric in Figure 34 where the warp yarns are cut and visible as dark lenticular shapes and the weft yarns winding up and down between the warp yarns. From this picture it is also evident that the crimping factor of both weft and warp yarns is roughly the same since the mid point of each warp yarn is slightly above or below the mid line of the fabric.

The yarns per centimeter where also counted using a microscope. A ruler was laid on top of the fabric and the yarns were counted in the warp and weft direction as can be seen exemplary in Figure 35. The measurements are listed below in Table 2.

Figure 34: Microscopic side view Denier 1000 fabric

Figure 35: Thread spacing measurement

4.3.2   Experiments

The fabric was tested in uniaxial tension tests to obtain the elastic properties to validate the model after the simulation took place. Figure 36 shows the Admet Uniaxial Material Test System used to obtain the load applied to the samples. The specimen is cut into rectangular samples parallel to the yarns with side lengths of 50 mm x 225 mm. These specimens are then clenched between the machines jaws to apply a force. The force is measured by a 1000 lbs rated load cell unit located behind the jaw. In the picture a white cable can be seen on the left side

	Yarn width [mm]	Yarn height [mm]	Yarn Spacing [yarns/cm]
Weft	0.635	0.25	10
Warp	0.635	0.25	13

Table 2: Geometric data of the fabric

to transmit the data to the computer. The specimen is pulled with a constant displacement rate of 1 inch per minute. The white speckle pattern visible in the photo allows the GOM Aramis DIC software to track the motion of the speckles. The sensors (cameras) of the software tracks the movement of the speckles at a rate of one image per second and compares each image to the original reference image to automatically compute the surface displacement and strain fields.
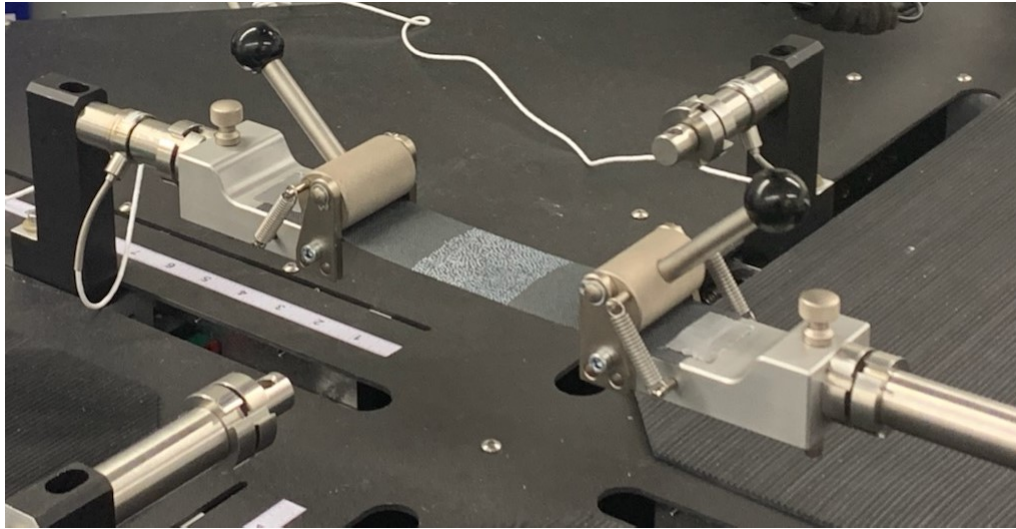
Figure 36: Uniaxial tension test of the fabric.

With utilization of the GOM DIC software in conjunction with the Admet Uniaxial Material Test System multiple stress-strain and strain-strain curves were acquired. The initial slope of the stress-strain curve was calculated to get the Young's Moduli in the warp and weft direction. The Poisson's ratio can be derived through the initial slope of the negative transverse strain over the axial strain.

The specimen was tested in both warp and weft direction to obtain the Young's moduli E_{11} and E_{22} respectively. With the same experiments the Poisson's ratio

ν_{12} and ν_{21} could also be measured. For the shear modulus G_{12} measurements, specimen were cut in an orientation where the yarns were oriented in a 45° angle towards the induced force and tested the same way. The averages of the measurements are shown in Table 3 below. These measurements are the initial slope of the stress strain curve. The initial slope is the first linear response of the material that can be compared to modelling results.

	$\mathbf{E_{11}}$	$\mathbf{E_{22}}$	ν_{12}	ν_{21}	$\mathbf{G_{12}}$
psi	35,126	15,948	0.912	0.846	88.7
MPa	242.185	109.958	0.912	0.846	0.612

Table 3: Averages of the fabric measurements in psi and MPa

To determine the yarn properties, Young's modulus was obtained by tension tests. One yarn was detached from the fabric and clamped into the test machine using specialized yarn grips. The resulting curve of the second run can be seen in Figure 37. The slope of the first, linear section was averaged over all the runs to get a good estimation of Young's modulus in the yarns directions. This average value was 0.9858 GPa. To calculate the stress a elliptical cross section of the yarn with the values of Table 2 were taken as major and minor diameters and were used to compute the yarn cross-sectional area. The engineering strain was calculated by dividing the change in length by the initial gage length of the yarn.
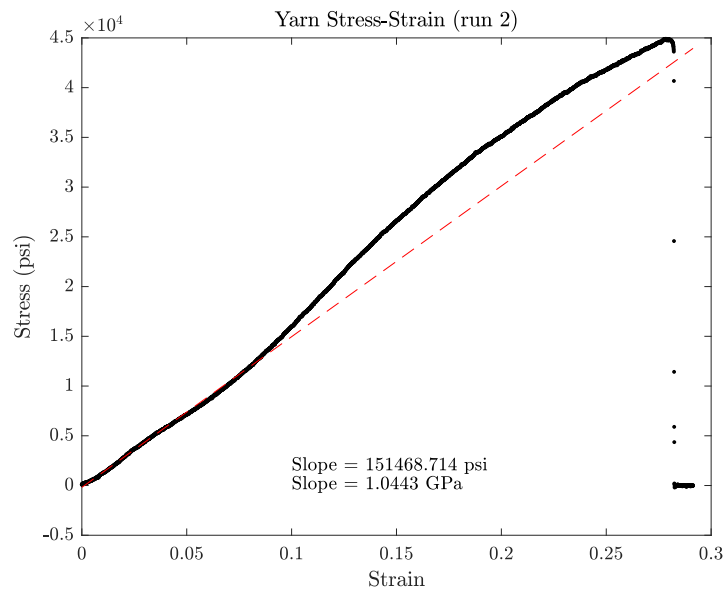
Figure 37: Stress strain curve of the yarn testing

4.4 Discussion

In the following section the simulation results and the experimental results are compared. The sensitivities of the different models will also be addressed.

Table 4 shows the list of the Young's modulus of the different simulation approaches and the experimental results. Since the measured fabric has a yarn density of 10 yarns per centimeter in weft and 13 yarns per centimeter in warp direction, the simulation results from section 4.1 are interpolated to give these results. The netting analysis gives the highest results, as shown in section 4.1,

	E_{Warp} $[MPa]$	E_{Weft} $[MPa]$	$\nu_{warp,weft}$	$\nu_{weft,warp}$
Experimental Results	242.185	109.958	0.912	0.846
Netting Analysis	290.000	220.000	-	-
Voxel Model	129.686	76.201	0.550	0.328
Dry Fiber Model	95.704	60.655	-	-

Table 4: Comparison of the simulation results with the experimental data

followed by the voxel model. The dry fiber model shows the lowest Young's moduli. While the netting analysis correlates well with the experimental results in warp direction, it overestimates the experimental results in weft direction, where both of the other models show more agreement. The simulated Poisson's ratio in the voxel model shows the same trend as the experimental results. The Poisson's ratio $\nu_{weft,warp}$ is lower than the Poisson's ratio $\nu_{warp,weft}$. But the simulated ratios are both lower than the measured, experimental ones. Since the experimental results exhibit a surprisingly high variation, new measurements are planned to verify the accuracy of these measurements.

The simulation results are highly dependant on the transverse and shear moduli of the yarn, which can be adjusted to improve agreement with the experimental results. This dependence can be seen in Table 5 and Table 6. These tables show a trial and error voxel study where the transverse and shear moduli are varied. For this study it is assumed that $E_{22} = E_{33}$ and $G_{12} = G_{13} = G_{23}$. A change in one, or

Case number	1	2	3	4	5
transverse moduli [Pa]	1.00E+04	1.00E+06	1.00E+04	1.00E+08	1.00E+08
shear moduli [Pa]	1.00E+04	1.00E+10	1.00E+12	1.00E+08	1.00E+09
E_{weft} [Pa]	2.84E+04	3.74E+07	2.19E+08	1.06E+08	1.49E+08
E_{warp} [Pa]	8.31E+04	7.36E+07	2.56E+08	1.58E+08	1.89E+08
$\nu_{weft,warp}$	0.425	0.477	0.0729	0.253	0.195
$\nu_{warp,weft}$	1.24	0.939	0.0852	0.376	0.248

Table 5: Results of the test cases 1 through 5

Case number	6	7	8	9	10
transverse moduli [Pa]	1.00E+07	1.00E+02	1.00E+08	1.00E+09	1.00E+09
shear moduli [Pa]	1.00E+09	1.00E+12	1.00E+06	1.00E+06	1.00E+07
E_{weft} [Pa]	6.95E+07	2.19E+08	6.91E+06	8.28E+06	5.30E+07
E_{warp} [Pa]	1.14E+08	2.56E+08	1.99E+07	2.32E+07	1.03E+08
$\nu_{weft,warp}$	0.342	0.0729	0.523	0.530	0.414
$\nu_{warp,weft}$	0.560	0.0852	1.51	1.48	0.804

Table 6: Results of the test cases 6 through 10

both of these values has a huge impact on the measured Young's modulus in both direction as well as the Poisson's ratio. The same dependence of transverse and shear properties can be observed in the dry fiber models. An adjustment of those data can give a better correlation between the simulated data and the experimental measurements. From the Tables 5 and 6, it can also be seen that the unusual high Poisson's ratio can be obtained with an appropriate choice of transverse and shear moduli.

CHAPTER 5

Conclusions and Future Research

5.1 Conclusions

This thesis demonstrates the ability to model complex geometrical structures of woven fabrics in Abaqus finite element simulations using the TexGen program to generate geometric models. The geometry of the woven structures can be altered easily to represent a variety of different weaves. In addition to the geometric modelling, this thesis shows that it is possible to determine the linear elastic response of these woven fabrics under small displacements with the voxel model. The challenges associated with validating the results of the simulation are highlighted.

It is also discovered, that larger displacements can be modeled with a dry fiber model and material properties can be extracted. Even complicated stress cases with differing multiaxial stress states can be simulated. The validation of these models reveal further challenges.

Most of the recent work in homogenizing materials and extracting material properties is done with composites where the matrix dominates the transverse and shear response of the material. In contrast to the composite material, the effect of transverse and shear moduli of the yarn in dry fiber simulation are crucial to accurately predict woven fabric behavior. These moduli were underestimated in this thesis which lead to inconclusive results. Nonetheless, this thesis highlights which parameters need to be examined more carefully when conducting dry fiber simulations and experiments.

5.2 Future Research

In subsequent research a variety of areas require further investigation. The most important advancement in these simulations is the correct determination of

the yarn's transverse and shear properties. To determine these properties experimentally is immensely challenging. A automated study to run different cases with different values as described in chapter 4 may be the easiest and fastest way to determine these moduli. To automate such a study, two approaches would improve the efficiency of the models. The first way is to run the EasyPBC plugin with a script to calculate more variations of properties faster. The current implementation of EasyPBC requires manual submission of job through Abaqus CAE. The second way is to use the Isight tool in Abaqus. Isight is a tool which can automatically vary input data and iterate the program code to find a desirable solution [1].

Another improvement to the simulation results can be made by further investigating the geometric properties of the fabric. The more accurate the fabrics measurements are, the better it can be represented in a model. The same is true for the Young's modulus of the yarn. A more refined testing technique and more test data may be able to more accurately determine the Young's modulus of the yarn and would further improve the simulation.

Once a validated data set is found for all needed properties, this data can be inserted into the dry fiber model to further verify the voxel model and simulate the nonlinear woven fabric material response. This approach can then be used as a design tool for use in the selection of appropriate fabrics for use in textile structures.

List of References

[1] Dassault Systemes. "Isight." July 2021. [Online]. Available: https://www.3ds.com/products-services/simulia/products/isight-simulia-execution-engine/

BIBLIOGRAPHY

Abaqus/Simulink. "Abaqus documentation." July 2021. [Online]. Available: https://abaqus-docs.mit.edu/2017/English/SIMACAEEXCRefMap/ simaexc-c-docproc.htme

Alich, A. M., "Modeling, simulation and investigation of inflatable drop-stitch panels with finite element analysis," Master's thesis, University of Rhode Island (URI), 2019.

Altenbach, H., *Kontinuumsmechanik.* Springer, 2012.

Bäker, M., "Numerische methoden in der materialwissenschaft," 2009.

Beccarelli, P., *Biaxial testing for fabrics and foils: Optimizing devices and procedures.* Springer, 2015.

Buet-Gautier, K. and Boisse, P., "Experimental analysis and modeling of biaxial mechanical behavior of woven composite reinforcements," *Experimental mechanics*, vol. 41, no. 3, pp. 260–269, 2001.

Cavallaro, P. V., Sadegh, A. M., and Quigley, C. J., "Decrimping behavior of uncoated plain-woven fabrics subjected to combined biaxial tension and shear stresses," *Textile Research Journal*, vol. 77, no. 6, pp. 403–416, 2007.

Cherif, C. *et al.*, *Textile Werkstoffe für den Leichtbau.* Springer, 2011.

Chu, T., Ranson, W., and Sutton, M. A., "Applications of digital-image-correlation techniques to experimental mechanics," *Experimental mechanics*, vol. 25, no. 3, pp. 232–244, 1985.

Dassault Systemes. "Isight." July 2021. [Online]. Available: https://www.3ds. com/products-services/simulia/products/isight-simulia-execution-engine/

Gager, J. and Pettermann, H., "Fem modeling of multilayered textile composites based on shell elements," *Composites Part B: Engineering*, vol. 77, pp. 46–51, 2015.

Hanabusa, Y., Takizawa, H., and Kuwabara, T., "Numerical verification of a biaxial tensile test method using a cruciform specimen," *Journal of Materials Processing Technology*, vol. 213, no. 6, pp. 961–970, 2013.

Horrocks, A. R. and Anand, S. C., *Handbook of technical textiles.* Elsevier, 2000.

Logan, D. L., *A first course in the finite element method.* Cengage Learning, 2016.

McCormick, N. and Lord, J., "Digital image correlation," *Materials today*, vol. 13, no. 12, pp. 52–54, 2010.

Misra, R., Dixit, A., and Mali, H. S., "Finite element (fe) shear modeling of woven fabric textile composite," *Procedia materials science*, vol. 6, pp. 1344–1350, 2014.

Omairey, S. L., Dunning, P. D., and Sriramula, S., "Development of an abaqus plugin tool for periodic rve homogenisation," *Engineering with Computers*, vol. 35, no. 2, pp. 567–577, 2019.

Peters, S. T., *Composite filament winding*. ASM International, 2011.

Sadd, M. H., *Elasticity: theory, applications, and numerics*. Academic Press, 2009.

Shahzamanian, M., Tadepalli, T., Rajendran, A., Hodo, W. D., Mohan, R., Valisetty, R., Chung, P., and Ramsey, J., "Representative volume element based modeling of cementitious materials," *Journal of engineering materials and technology*, vol. 136, no. 1, 2014.

Sherburn, M., "Geometric and mechanical modelling of textiles," Ph.D. dissertation, University of Nottingham Nottingham, UK, 2007.

University of Nottingham. "Texgen." June 2021. [Online]. Available: http://texgen.sourceforge.net/index.php/Main_Page

Ye, F. and Wang, H., "A simple python code for computing effective properties of 2d and 3d representative volume element under periodic boundary conditions," *arXiv preprint arXiv:1703.03930*, 2017.

Yoneyama, S. and Murasawa, G., "Digital image correlation," *Experimental mechanics*, vol. 207, 2009.